Science of the Total Environment 781 (2021) 146706

Contents lists available at ScienceDirect

Science of the Total Environment

journal homepage: www.elsevier.com/locate/scitotenv

An evapotranspiration model driven by remote sensing data for assessing groundwater resource in karst watershed

Chloé Ollivier [a,b,*], Albert Olioso [b], Simon Damien Carrière [b,c], Gilles Boulet [a], Konstantinos Chalikakis [b], André Chanzy [b], Jean-Baptiste Charlier [d,g], David Combemale [b,e], Hendrik Davi [f], Christophe Emblanch [b], Olivier Marloie [f], Nicolas Martin-StPaul [f], Naomi Mazzilli [b], Guillaume Simioni [f], Marie Weiss [b]

[a] CESBIO, Université de Toulouse, CNES,CNRS, INRAE, IRD, UT3, Toulouse, France
[b] EMMAH, INRAE, Avignon Université, Avignon, France
[c] METIS, Sorbonne Université, UPMC, CNRS, EPHE, Paris, France
[d] BRGM, Université Montpellier, Montpellier, France
[e] SILVA, Université de Lorraine, AgroParisTech, INRAE, Nancy, France
[f] URFM, INRAE, Centre de recherche PACA, Avignon, France
[g] G-eau, INRAE, CIRAD, IRD, AgroParisTech, Institut Agro, BRGM, Montpellier, France

HIGHLIGHTS

- SimpKcET (Simple Crop coefficient for Evapotranspiration) reproduces the dynamics of ET of a wide range of vegetation cover
- A better estimation of ET with SimpKcET of a large watershed improves simulations of its outflow discharges.
- The shading of the soil by the presence of pieces of rock on its surface limits the evaporation, this process plays a major role in the estimation of ET.
- Despite the simplicity of the assumptions, the estimates are below 0.5 mm. d^{-1}.

GRAPHICAL ABSTRACT

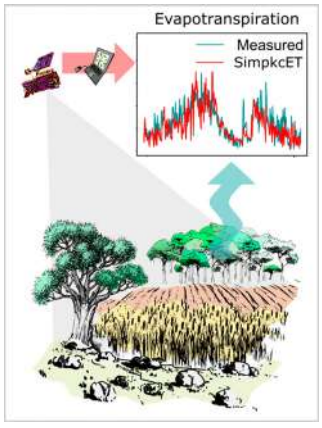

ARTICLE INFO

Article history:
Received 7 January 2021
Received in revised form 15 March 2021
Accepted 19 March 2021
Available online 25 March 2021

Editor: Christian Herrera

Keywords:
Evapotranspiration
Fraction cover
Hydrological modelling

ABSTRACT

Aquifer recharge may depend mainly on the difference between precipitation and evapotranspiration. Hydrological models used to estimate groundwater reserves use evapotranspiration models that are mainly determined by climate demand. In particular, mechanisms of plant transpiration are neglected, although transpiration constitutes 70% of evapotranspiration. This is problematic when considering karst watershed, which are poorly documented at the interface between soil and atmosphere where vegetation and soil properties control water flows. To fill this gap, we propose an evapotranspiration model that integrates the processes of plant transpiration and soil evaporation. The dynamics of vegetation is evaluated using the Enhanced Vegetation Indexes from the Terra and Aqua Moderate Resolution Imaging Spectroradiometers. The soil evaporation calculation account for the impact of coarse elements at soil surface. The "Simple Crop coefficient for Evapotranspiration" (SimpKcET) model is tested at flux tower sites over forest of Font-Blanche, Puechabon and the agricultural area of Avignon. The simulated daily evapotranspirations are very close to the observations (RMSE ~0.5 mm.d^{-1}), while the model is simple compared to other models proposed in the literature. The SimpKcET is implemented in a karst hydrological model to evaluate the impact of evapotranspiration estimation on the aquifer flow rate simulation. This approach

* Corresponding author at: CESBIO, Université de Toulouse, CNES, CNRS, INRAE, IRD, UT3, 18 Avenue Edouard Belin, 31401 Toulouse, France.
E-mail address: chloe.ollivier@ird.fr (C. Ollivier).

https://doi.org/10.1016/j.scitotenv.2021.146706

Karst
Recharge

is applied to the vast watershed of Fontaine de Vaucluse. In comparison to the water bucket model that is frequently used in karst models, SimpKcET provide ET simulations that are more in line with ET processes. A cross wavelet analysis highlighted the improvement of the simulated recharge and observed flow rate relationship brought by the consideration of evaporation and transpiration processes. The use of remote sensing data related to plant activity makes it possible to propose a parsimonious model that can be applied to all types of vegetation (agricultural, natural, mixed forest) and that can be transferred to other karst models.

1. Introduction

An accurate knowledge of aquifer recharge is determinant for water resources assessments. Aquifer recharge is the quantity of water which supplies underground reserves. It mainly results from the infiltrated amount of the difference between precipitations (P) and evapotranspiration (ET), that both vary in space and time. ET is a difficult term to quantify [Shuttleworth, 2007; Farahani et al., 2007]. Thus, a poor estimate of ET can have a strong impact on the assessment of the spatial distribution of aquifer recharge. When considering karst aquifers that have complex hydrodynamic properties, knowledge of the distribution of evapotranspiration and recharge is even more difficult.

ET is the sum of water transpired by the plants and the water evaporated by other surfaces as soil surface and free water [Shuttleworth, 2007]. It depends on many factors related to climate, vegetation and soil. ET is a major process in the water cycle. It consumes around two-thirds of the world terrestrial rainfall according to McDonald [1961] and Brutsaert [1982]. Despite its importance, ET is still poorly quantified as it is complex and expensive to measure [Rana and Katerji, 2000; Shuttleworth, 2008]. ET processes are difficult to model as the variability of ecosystem response to climate and soil moisture is large. ET models intercomparing exercises [Grippa et al., 2017; Kimball et al., 2017] show that simulated ET exhibit large differences from one model to another.

In most karst hydrogeological studies, ET processes are highly simplified. In particular, models used to evaluate water resources often neglect the transpiration dynamics of plants [Hartmann et al., 2015; Hartmann et al., 2012; Oudin, 2004]. This may have large implications on the dynamics of simulated ET and thus, simulated recharge. In the current context of global changes, it is important that the interactions between land cover and climate evolutions can be described in a realistic way [Breshears et al., 2005; Cramer et al., 2001; Liu et al., 2019]. Therefore, it is important to model ET that represent the most important term of water cycle after Fisher et al. [2017] and ET is at the heart of climate – land surface interactions.

Hydrological models are constructed from a water balance equation, assuming that water inputs (mainly due to precipitations) are equilibrated by water outputs (ET, runoff from streams and springs) and storage variations. In many cases, adjustment variables for obtaining this equilibrium are groundwater stock and ET. The estimation of ET in hydrogeological models is often constrained by the optimisation of the rainfall-discharge relationship. For instance, Oudin et al. [2005a, 2005b] studied the importance of ET formulation in numerous rainfall-discharge models. They showed that even large variations in ET produced only small variations in simulated flow rate. Actually, the calibration of model parameters compensated for the differences in ET inputs. It should be noted that these models were not accounting for spatial variations of water flows, which has an impact on the simulation of global flow. Using a distributed model, Ollivier et al. [2020] showed that the location of precipitation has an impact on simulations of karst aquifer discharges. They argued that the spatial distribution of ET components should also have a significant impact and that an accurate estimation of both temporal evolution of ET and its variation in space could improve the simulation of flow rate. One of the improvements in hydrogeological modelling of karst systems would be the implementation of a model that better describes evapotranspiration and at the same time improves the relation between rainfall and discharge in karstic hydrosystems.

Direct ET measurements can be performed at local scale. The data from a large number of micrometeorological tower sites all over the world are compiled in the FLUXNET database [Baldocchi et al., 2001; Chu et al., 2017]. Micrometeorological tower relies on eddy covariance methods to measure the exchanges of carbon dioxide, water vapor and energy between terrestrial ecosystems and the atmosphere. They provide ET estimates at a specific location, for a given type of cover. These measures are strongly influenced by local environmental factors, and extrapolation to regional scales is difficult. However, these measurements provide insights into the daily dynamics of ET for specific ecosystems.

Spatially distributed information on vegetation activity and ET may be provided by satellite remote sensing. For example, the MODIS (Moderate Resolution Imaging Spectroradiometer) sensors on board of the Terra and the Aqua satellites are viewing the entire Earth's surface every day, acquiring data that are used to monitor vegetation and ET at spatial resolutions of 1 km [e.g. Allies et al., 2020; Gallego-Elvira et al., 2013; Mu et al., 2007]. In particular, the combination of the bands specific to the plant activity allows the calculation of vegetation indexes such as the Normalized Difference Vegetation Index (NDVI) and the Enhanced Vegetation Index (EVI) [Huete et al., 2010, 2002, 1994] and thus the monitoring of vegetation. Operational products based on remote sensing data, such as GLEAM [Martens et al., 2017] or MOD16 [Mu et al., 2007, 2011] are providing ET estimates at different scales (30 km every day and 1 km for 8 days periods, respectively). These products could be used for hydrological studies. However, they are still imperfect as they have drawbacks as either low spatial resolution, low time resolution or a strong uncertainty [e.g. Hu et al., 2015; Jung et al., 2019; Moreira et al., 2019; Shen et al., 2017; Zhang et al., 2018].

While remote sensing information is intensively used in various research fields, the integration of remote sensing data in groundwater modelling is not a very common practice yet In order to evaluate the benefit for water resource evaluation of an accurate estimation of ET, we proceed as follows:

- to propose an evapotranspiration model that enables a consistent representation of main processes (vegetation transpiration and soil evaporation),
- to develop an efficient model with available parameters for all types of vegetation,
- to evaluate the consistency of the proposed model against commonly used models into hydrogeological models of karst hydrosystem.

In this article we propose a remote sensing driven ET model that considers the transpiration dynamics of natural and agricultural vegetation cover and the evaporation of stony soils. The model can easily be integrated into hydrological models, herein called SimpKcET. The dynamics of vegetation covers is evaluated using vegetation indexes from MODIS dataset. We tested the SimpKcET model over three different types of vegetation cover for which ET measurements are available: two forest sites mostly constituted by sempervirens trees (*Quercus ilex* L. and *Pinus halepensis* Mill.) and a wheat crop site.

The SimpKcET model was integrated into a spatially distributed hydrological model dedicated to karst catchments in a second step (the KaRaMel model developed by Ollivier et al., 2020) for simulating water flows of karst aquifer. The test site is the karstic aquifer of the Fontaine de Vaucluse, located in Southeast of France. This aquifer has a watershed area of 1162 km^2 mainly occupied by forests and natural environments. The daily simulated ET of Fontaine de Vaucluse watershed is compared with ET simulated with a usual ET model often employed by hydrological modelling of karst aquifer. The influence of the ET model on the flow simulation is evaluated with a wavelet analysis.

2. Evapotranspiration model and karst model

2.1. Usual evapotranspiration model in karst groundwater models

Surface of karst system can be very heterogeneous, for instance karstic features induce an important variation of soils properties. Soils can be thick and clayey in dolines (enclosed karst depressions, called also sinkholes in some cases, e.g. Ford and Williams, 2007), thin and stony on slopes, and discontinuous when soil fills the deepest forms of lapiaz (a network of chiseling on the surface of compact carbonate, which can be from a few mm to 10 m deep; it is due either to the dissolution or erosion). Karstic features indicate the presence of an underlying karst aquifer with extensive solution channels crossing the unsaturated zone. Compared to common porous aquifers, the important anisotropy of the hydrodynamic properties of the unsaturated zone of the karst, limits the possibility to model subsurface flows and exchanges with the atmosphere with classical diffusivity equations. Therefore, karst is often represented with lumped models. Lumped approaches conceptualize the physical processes at coarse scale without modelling spatial variability explicitly. They are mostly based on linear or nonlinear relationships between rainfall and discharge [Fleury et al., 2007; Tritz et al., 2011]. The spatial variability of selected components can be represented with semi-distributed lumped models. The modelled hydrosystem is then subdivided into entities assumed to be homogeneous for the dominant characteristics [Kite and Kouwen, 1992]. This type of modelling is used to model karstic hydrosystems by considering different sources of heterogeneity such as precipitation regime and runoff processes [Bailly-Comte et al., 2012], transfer dynamics within the unsaturated zone [Ladouche et al., 2014; Ollivier et al., 2020] or evapotranspiration [Jódar et al., 2018; Sarrazin et al., 2018]. In common lumped karst models, the ground is represented by a single overflow storage (Fig. 1). The actual evapotranspiration (ET) is a direct function of the soil moisture state, and recharge (Q_H) occurs only when the infiltration water exceeds the soil available water capacity (SAWC) [e.g. Fleury et al., 2007; Rahman and Rosolem, 2017; Tritz et al., 2011; Ollivier et al., 2020]. In the present work, this simple modelling of evapotranspiration is referred to as the bucket model and used as reference.

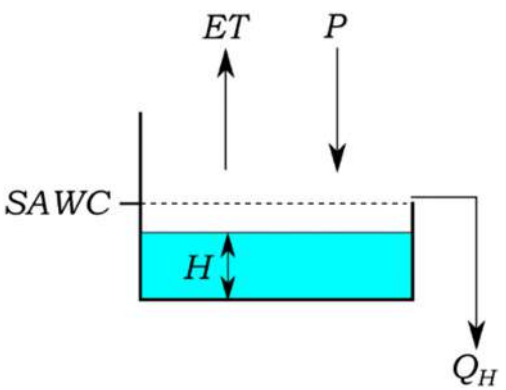

Fig. 1. Schema of the bucket model of evapotranspiration.

$$ET = \begin{cases} H + P, \text{ if } H + P < k.ETp \\ k.ETp, \text{ if } H + P \geq k.ETp \end{cases} \quad (1)$$

$$Q_H = \begin{cases} 0, \text{ if } H + P - ET < SAWC \\ P - ET, \text{ if } H + P - ET \geq SAWC \end{cases} \quad (2)$$

$$\frac{dH}{dt} = \begin{cases} \max(P - ET, 0), \text{ if } H < SAWC \\ P - ET - Q_H, \text{ if } H \geq SAWC \end{cases} \quad (3)$$

where ET is the daily evapotranspiration (in mm.d^{-1}), P the daily precipitation (in mm.d^{-1}), ETp the daily potential evapotranspiration corresponding to climate demand (in mm.d^{-1}). H is the water level of the reservoir (in mm), Q_H stands for daily infiltration and runoff (in mm), SAWC is the soil available water capacity (in mm). Evapotranspiration depends on climatic demand with a scaling coefficient (k). As in many hydrological karst models, Ollivier et al. [2020] set the scaling coefficient k to 1 [e.g. Fleury et al., 2007; Messerschmid et al., 2020]. ETp may be calculated with different methods depending on the study. Here we used the so-called reference evapotranspiration ETo as described in Section 2.2.

However, several studies proposed that k is not constant depending on surface conditions. For instance, Tritz et al. [2011] expressed k as a function of time, Charlier et al. [2012], Hartmann et al. [2012] and Perrin et al. [2003] as a function of reservoir fill rate in order to represent the soil resistance to evaporation. Coefficient k may also simulate a reduction in ET/ETo as the transpiration capacity of plants may be limited by plant development and plant access to available water in the soil [Sarrazin et al., 2018; Jódar et al., 2018]. Sarrazin et al. [2018] implemented a physically based evapotranspiration equation into a semi-distributed lumped model of epikarst. They used the average leaf area index and an extinction coefficient to estimate the canopy cover fraction and to separate the evapotranspiration flux into transpiration and evaporation. Their model depends on many parameters for describing the vegetation (LAI, vegetation height, stomatal resistance) and the soil (soil resistance, storage capacity of soil layers), which limits the application at large scale. However, their work points out that better modelling of evapotranspiration in karst hydrological models is needed to forecast the impact of vegetation change on resources. Jódar et al. [2018] showed that remote sensing can be used to assess the spatial variations of k in relation to plant development.

2.2. Remote sensing-based model to estimate evapotranspiration, SimpKcET

In this study we proposed to improve the simulation of ET by using the SimpKcET model which considers that ET depends on the climatic demand, the dynamics of the vegetation, which is monitored using remote sensing data, the level of soil moisture in the root zone and the fraction of rocks and coarse elements in the surface soil layer. Standard evapotranspiration models (like the FAO56 method) consider the lack of evaporation from soils under plant canopies, but they neglect the reduction of evaporation from soils by pebbles and rocks in the surface layer. In the case of soils growing on carbonate bedrock, the presence of pebbles or denudated rocks is significant [Bottner, 1971; Godard et al., 2016] as shown for instance on the aerial photography in Appendix C, Figure C-1:.

SimpKcET basically follows the "dual crop coefficient (under non-standard conditions)" proposition given by Allen et al. [1998] with some simplifications. These simplifications were justified by the low level of information available for computing ET from natural areas (ecosystem composition and heterogeneity, soil characteristics…). In comparison, information related to agricultural vegetation is more abundant because they are needed for the evaluation of water

requirements, in particular for irrigation management, and crop productivity. ET is thus expressed using the following equation:

$$ET = k_C * ETo \quad (4)$$

The coefficient k_C (-), equivalent to the classical crop coefficient, was composed of two terms, k_T (-) the canopy transpiration coefficient and k_E (-), the soil evaporation coefficient:

$$k_C = k_T + k_E \quad (5)$$

The reference evapotranspiration (ETo) corresponds to ET that would be produced by a well irrigated grass surface. ETo is computed using the Penman-Monteith equation as proposed by Jensen et al. [1990] and Allen et al. [1998]. Other equations such as Penman equation or Hargreaves equation have been widely used to represent climatic demand [e.g. Doorenbos and Pruitt, 1977; Hargreaves and Samani, 1985; Oudin et al., 2005b; Trajkovic, 2005], but the Penman-Monteith equation is considered as better suited for accounting for vegetation processes [Allen et al., 1998; Hargreaves and Allen, 2003]. It expresses ETo with the following formula:

$$ETo = \frac{\Delta * (R_n - G) + \rho_a * c_p * \frac{VPD}{r_a}}{L\left[\Delta + \gamma * \left(1 + \frac{r_s}{r_a}\right)\right]} \quad (6)$$

where Δ is the slope of the vapor pressure saturation curve, ρ_a the density of the air, c_p the specific heat of the air at constant pressure, γ the psychrometric constant and L the latent heat of vaporization. The term r_a represents the aerodynamic resistance while the term r_s is the surface resistance which corresponds to the integration of stomatal and soil surface resistance. R_n and G are the net radiation and the ground heat flux. Their difference represents the energy available for ET. VPD is the Vapor Pressure Deficit in the air above the surface. Specific values of the parameters to compute the resistance terms and the available energy were defined for reference types of canopy such as clipped grass or alfalfa stand. A full description of the ways to use this equation for reference evapotranspiration computing is given by Allen et al. [1998].

The canopy transpiration coefficient (k_T) is related to both vegetation amount and water stress. We use the fraction of vegetation cover f_{cover} that can be easily derived from remote sensing data using vegetation indices or neural network models as a proxy of vegetation amount. The canopy transpiration coefficient k_T can thus be expressed as:

$$k_T = f_{cover} * k_s * k_{Tx} \quad (7)$$

where k_{Tx} is the maximum value of the canopy transpiration coefficient and k_S the water stress depending on soil moisture (Fig. 2). Classical values for k_{Tx} range between 0.8 and 1.5 depending on the vegetation type and the definition of ETo. Strong relations between f_{cover} and k_T (or k_C when soil evaporation was insignificant) were obtained in various studies [e.g. Heilman et al., 1982; Melton et al., 2012] and analysed theoretically by Choudhury et al. [1994] and Allen and Pereira [2009]. Their results showed that, even if the k_T (f_{cover}) relation can be curvilinear, a linear relationship can be generally considered as an acceptable approximation. The water stress coefficient k_S is expressed as a function of the root zone water availability as presented in Fig. 2. The root zone water availability is defined as the ratio of available water to SAWC representing the maximum amount of water that can be available for ET. The water stress coefficient is set to 1 for root zone water availability larger than 2/3. Below this threshold, it linearly decreases to zero with the water availability.

The soil evaporation coefficient k_E accounts for the evaporation processes that occur over the fraction of soil that is not covered with vegetation (1-f_{cover}), bulk elements and rocks (1-f_{rocks}):

$$k_E = (1 - f_{cover}) * (1 - f_{rocks}) * k_{ini} \quad (8)$$

where the coefficient k_{ini} is equivalent to the initial stage crop coefficient defined by Allen et al. [1998] and Allen et al. [2005] for representing the soil evaporation at the beginning of crop growth. It expresses the capacity of the soil surface layer to evaporate depending on the climatic demand (ETo) and the frequency of rainfall events (Fig. 3). It is expressed as:

$$k_{ini} = \left[1 + \left(\frac{ETo}{a}\right)^b\right]^{-1} \quad (9)$$

where a is the number of rainy days in the last 20 days and b is a coefficient expressing the availability of water to evaporation. This parameter was calibrated so that the shape of k_{ini} globally matches the curves presented in Allen et al. [1998]. Its value ranged between 1 and 5.

Once again, more complex descriptions of k_s and k_{ini} were proposed by Allen et al. [1998] and Allen et al. [2005] and for example used by Jódar et al. [2018]. However, to be applied, they require a precise knowledge of plant types and soil types which is not usually available over large areas or for complex systems, such as soil in karst systems and epikarst.

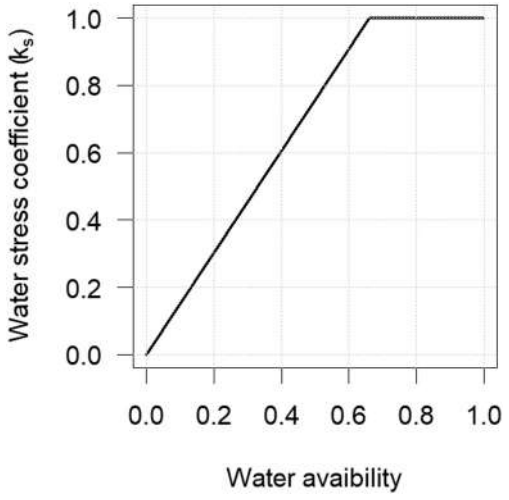

Fig. 2. Relationship between the water stress coefficient (k_S) and the root zone water availability.

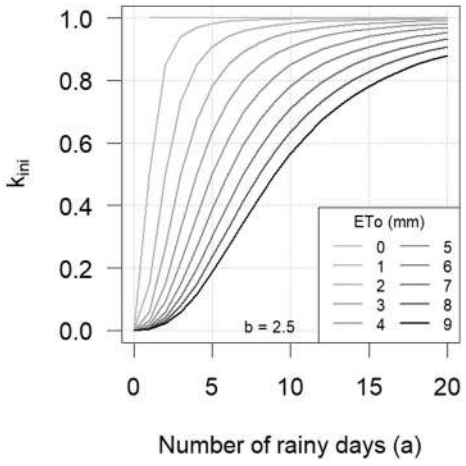

Fig. 3. Average k_{ini} as a function of the climatic demand (ETo) and the number of rainy days during the last 20 days (a) after Allen et al. [1998].

2.3. The karst model

The main characteristic of karst systems is a high degree of heterogeneities. The karst network features act as pipes and enable a rapid infiltration and then percolation of surface water to groundwater table. The karst network is developed through carbonate rock with very low hydraulic permeability. An important amount of water undergoes diffuse percolation through carbonate altered by fractures, diaclases and faults. The strong heterogeneity of karst formations makes it difficult to apply a distributed model to estimate the spatial distribution of water resources [Hartmann et al., 2014]. The Karst Recharge and discharge Model (KaRaMel) was developed from the consideration that knowledge of karst aquifer properties decreases with depth [Ollivier et al., 2020]. KaRaMel simulates the distribution of terrestrial water balance using a daily temporal resolution. Its structure considers infiltration of rainfall and snowmelt, ET and downward percolation from the upper soil layer to the underlying aquifer. Underground flows are represented with coarse resolution by a lumped model. A basic description of parameters of KaRaMel is given in the Appendix A.

The terrestrial water balance is controlled by the soil available water capacity (SAWC). SAWC is mapped over the watershed after soil measurements and a spatial interpolation method based on the principles of digital soil mapping [McBratney et al., 2003]. Underground flows are discretized into two classes: rapid and slow. The proportion of rapid to slow flows is controlled by the intrinsic vulnerability indices, based on the assumption that rapid flows through the vadose zone are dominant on areas with high karst features density. The consideration of these two levels of distribution of the parameters allows the simulation of the spatial variability of the hydrosystem stocks and the discharge at the aquifer outlet. Different ET models may be easily implemented into KaRaMel. We thus use KaRaMel to enable the evaluation of the consistency of the simulated input-output relationship of the karst system for the two different ET models: the bucket model (ETbu) and the SimpKcET model (ETsimp).

3. Data and model implementation

3.1. Test sites

SimpKcET was first evaluated over three local sites equipped with a micrometeorological tower and in a second time at the level of the karst aquifer of the Fontaine de Vaucluse system, the local sites cover different land uses under a Mediterranean climate. Two sites are forested areas: one oak forest, one oak and Aleppo pines mixed forest, both sites develop on carbonate rocks. The third site is a crop field (wheat) and is in an alluvial plain. The three local sites differed from the Fontaine de Vaucluse watershed by lower elevations and by being closer to the seaside (Fig. 4), which implied significant differences in rainfall and ETo (Appendix D).

3.1.1. The Font-Blanche forest

The Font-Blanche long-term experimental monitoring site is located in a mixed Mediterranean forest in south-eastern France (43°14′27″N, 5°40′45″E; altitude 425 m), 20 km east of Marseille (Fig. 4). It is dominated by Aleppo pines (*Pinus halepensis*) in the upper tree stratum (average height, 13 m) and holm oak (*Quercus ilex*) in the intermediate tree stratum (average height, 5 m). The understorey is composed of different species, mainly narrow-leaved mock privet (*Phillyrea angustifolia*) and kermes oak (*Quercus coccifera*) [Girard et al., 2012]. The climate is Mediterranean with hot, dry summers. The mean annual temperature and precipitation were 14 °C and 701 mm, respectively, between 2008 and 2017. The bedrock is karstified Cretaceous limestone. The soil has a maximum depth of around 50 cm, and a volumetric rock fraction of about 50% at the top, and up to 90% at the bottom.

Font-Blanche is part of the Integrated Carbon Observation System [ICOS, 2021] and the Analysis and Experiments on Ecosystems [AnaEE, 2021; see Clobert et al., 2018] networks. The site is equipped with a 17 m eddy-covariance flux tower on top of which meteorological variables (including radiation, rainfall, temperature, vapor pressure deficit), and carbon, water and energy fluxes are continuously monitored at 30 min intervals.

The available water capacity for plants used by Marie and Simioni [2014] in a modelling study was set to 145 mm. A more recent estimate based on the analysis of eddy covariance fluxes during the summer period is about 170 mm [Simioni et al., 2016]. The stone-free fine fraction of the soil is a homogeneous silty clay loam that contains around a third of the available water capacity (as observed from soil pit). The remaining extractable water is located in the subsoil (bedrock), within fractures and clay pockets.

3.1.2. The Puechabon forest

The Puechabon forest is located 35 km northwest from Montpellier (43°75′N, 3°6′E, 250 m. a.s.l.). The site and the data were described by Rambal [1992, 1993], Rambal et al. [2003], Allard et al. [2008] and Rambal et al. [2014]. It is located over a flat plateau and it is mainly composed of holm oak (*Quercus ilex*) of 5 m high. The understory is composed of sparse scrubs of 2 m height. The soil layer is developed into a limestone altered zone where the fine earth is composed of silt (35%), clay (39%) and sand (26%). The soil thickness ranges from 0 to 0.9 m but the soil content has a high proportion of stones and rocks (75% between 0 and 0.5 cm; 90% or more below). The plant roots are developed through soil pockets and explored limestone fissures. A large fraction of

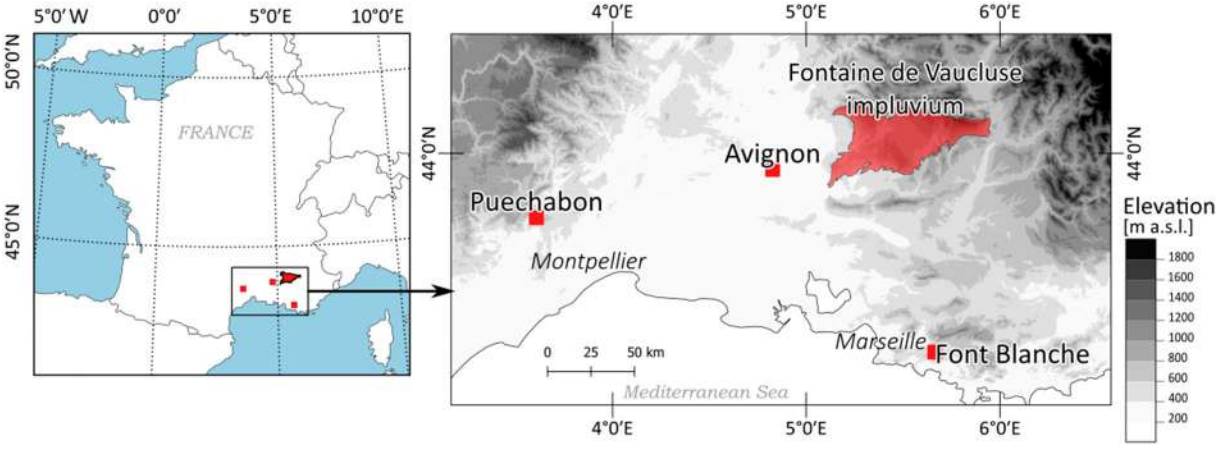

Fig. 4. The three test sites equipped with micrometeorological tower (red square) and the Fontaine de Vaucluse watershed (red polygon), located South-East of France. (For interpretation of the references to colour in this figure legend, the reader is referred to the web version of this article.)

the root mass is found in the first 0.5 m but some roots have been found down to a depth of 4.5 m.

The site was part of the CARBOEUROPE-IP [CARBOEUROPE-IP, 2019] European project and the data between 2000 and 2014 are available within the FLUXNET database ORNLDAAC2017. ET was derived from eddy covariance measurements of latent heat flux.

3.1.3. The Avignon crop site

Avignon crop site is located close to Avignon city (43°44′N, 4°5′E, 32 m a.s.l.). The site and the measurement setup were described by Garrigues et al. [2018, 2015]. The crop rotation consists in a succession of winter crops such as wheat and summer crops as maize or sunflower. During the inter-crop, no vegetation is usually present, the soil being ploughed sometime after the harvest. The soil is well developed with a thickness between 1.3 and 2.0 m. Its fine fraction is composed by clay (33%), sand (14%) and silt (53%). The underlying rock consists of alluvial deposits. Plant roots are developed through the soil down to more than 1.5 m in the case of wheat which resulted in SAWC between 170 and 230 mm [Garrigues et al., 2015].

The INRAE Avignon "Remote sensing and flux site" records acquired between 2015 and 2017 on two successive wheat crops were used in this work. Daily ET was obtained from latent heat flux measurements with the eddy-covariance method.

3.1.4. The Fontaine de Vaucluse aquifer

The Fontaine de Vaucluse spring is located South-East of France, about 40 km eastward of Avignon city (Fig. 4). The Fontaine de Vaucluse is one of the biggest karst springs in the world [Chen et al., 2017]. It is the only outlet of a karstic system with an exceptional extension of 1162 km^2 developed within a major relief of the Provence area [Carrière et al., 2016]. Geological and karstic features were mapped in Ollivier et al. [2020]. The Mont-Ventoux summit (1912 m a.s.l.) at the West and the Lure summit at the East (1826 m a.s.l.), delineate a 62 km long mountain chain that defines the northern boundary of the watershed. The main part of the watershed corresponds to highland with a mean elevation of 850 m. It is bounded on the East by the Durance river valley, on the South by the plains of Apt and on the West by the Rhone river valley. The landscape is mainly composed of natural area (84%), 15% is agricultural area and about 1% is urbanized. Natural areas include 52% of hardwood forests (holm oak, beeches, deciduous oak, chestnut…), 13% of coniferous forests (mountain pine, black pine, Corsican pine) and 7% of mixed forests (Fig. 5). Scrublands, lawns and natural pasture, shrub and sparse vegetation cover 27% of the area. Rock outcrops are visible over less than 1% of the studied area. Soils are well developed over cultivated fields, and they are really stony and thin over natural areas.

The absence of permanent rivers over the recharge area is a strong clue that most of surface water infiltrates and percolates to the groundwater. Therefore, it is possible to assume that most of the difference between rainfall and recharge is due to ET. Because of the large variety of land cover and soil, a large spatial variability of ET is expected over the studied area.

Fontaine de Vaucluse discharge has been monitored since November 2003 by a gauging station installed in the river, 450 m downstream of the spring. Water levels have been recorded every hour and converted into hourly discharge using the station's calibration curve [Ollivier, 2019]. In this study we use daily discharge data from November 2003 to August 2015. Over this period, discharge ranged from 2.8 to 82.5 m^3.s^{-1}, with an average of 13.2 m^3.s^{-1} and a median of 9.7 m^3.s^{-1} (Appendix A).

A soil available water capacity map of the top soil layer ($SAWC_0$) was developed after 323 soil pits observations spread over the watershed area. In Ollivier et al. [2020] an Artificial Neural Networks (ANN) was used to predict soil water holding capacity over the watershed area from environmental factors such as elevation, mountain side orientation, slope and vegetation amount The $SAWC_0$ map has a resolution of 1 km^2 and $SAWC_0$ values range from 5 mm (limestone outcrop) to 240 mm (agricultural area). RMSE between the simulations and observations was 17 mm for natural areas and 13 mm for agricultural areas.

3.2. Climate data

The climate data came from the SAFRAN product of METEO-FRANCE, the French meteorological service [Durand et al., 2009; Quintana-Seguí et al., 2008]. SAFRAN is a weather data source available over France on a grid of 8 km by 8 km at the daily scale starting in 1958. Precipitation and

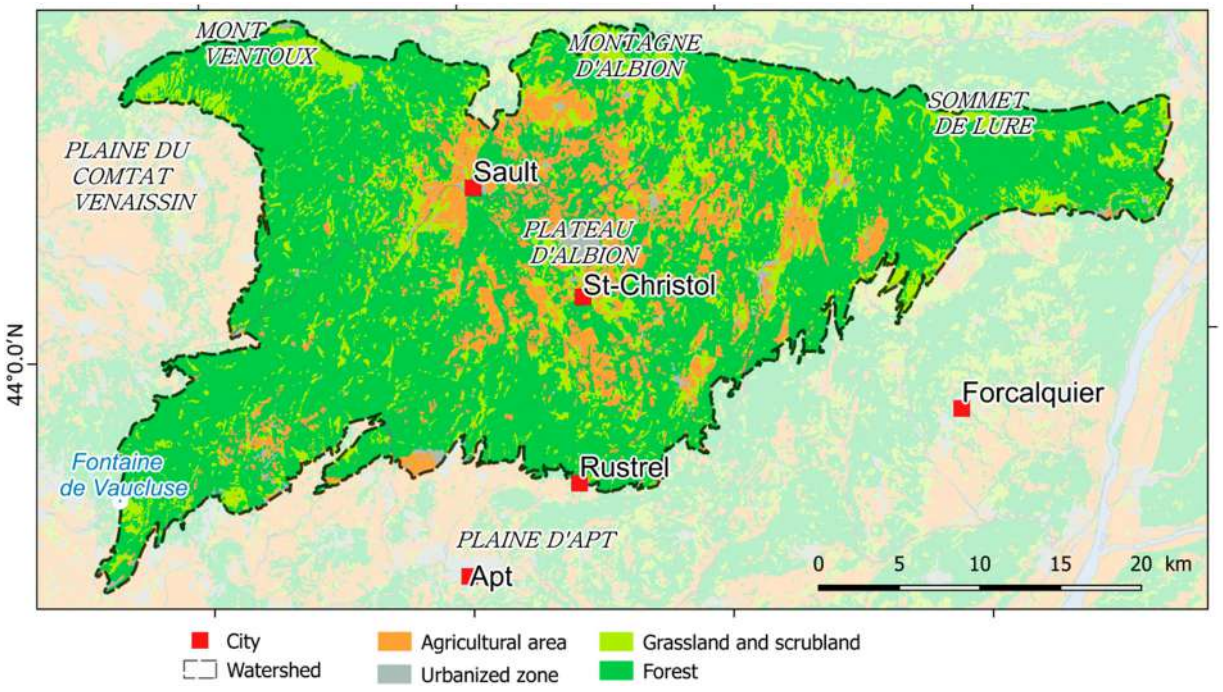

Fig. 5. Land use and land cover of the watershed of Fontaine de Vaucluse aquifer, after OCSOL-2014 data produced by the CRIGE-PACA (www.crige-paca.org).

Table 1
Remote sensing data product used to compute f_{cover} of Puechabon, Font-Blanche, Avignon and Fontaine de Vaucluse sites.

Site	Sensor	Resolution	Method	Product name
Puechabon	MODIS (Terra)	250 m and 500 m	Linear EVI	MOD13Q1.006 MOD13Q1.005
Font-Blanche	MODIS (Terra)	250 m and 500 m	Linear EVI	MOD13Q1.006 MOD13Q1.005
Avignon	Sentinel-2	20 m	Neural Net	S2_FCOVER
Fontaine de Vaucluse Watershed	MODIS (Terra)	1000 m	Linear EVI	MOD13Q1.005 tile h18v04

reference evapotranspiration data from SAFRAN are used, see details in Appendix D.

The four test sites are situated in the typical Mediterranean climate zone (Köppen-Geiger climate classification updated by Beck et al. [2018]). Winter is wet and cool, summer is hot and dry. Most of the precipitations occur during autumn and winter. Thus, climate is characterized by frequent summer droughts lasting at least for 2 months and regularly up to 4 months. Mean annual precipitation and temperatures of hydrological year from September 2000 to August 2016 are (Fig. D-1): 981 mm and 10 °C over Fontaine de Vaucluse watershed, 686 mm and 14 °C in Font-Blanche, 807 mm and 14.5 °C in Puechabon, 666 mm and 15 °C in Avignon. Mean annual reference evapotranspiration is 1043 mm for Fontaine de Vaucluse watershed, 1184 mm in Font-Blanche, 1213 mm in Puechabon and 1248 mm in Avignon. The difference in climatic demands between these sites is mainly related to temperatures. It is interesting to note that years with lowest precipitation amounts are characterized by highest reference evapotranspiration values. The interannual variability of reference evapotranspiration is very low (maximum range around 200 mm) compared to precipitation (maximum range around 700 mm).

3.3. Remote sensing data and fraction cover

Remote sensing data were used to calculate the fraction of vegetation cover which was used as input into the ET model. The fraction of vegetation cover (f_{cover}) represents the amount of land surface covered by vegetation.

f_{cover} is well related to vegetation indices that consist in combinations of spectral reflectance obtained from remote sensing images [e.g. Carlson and Ripley, 1997; Qi et al., 1994]. f_{cover} can also be obtained from other remote sensing products and in particular derived using artificial neural network (ANN) models [Li et al., 2015; Vuolo et al., 2016; Weiss et al., 2002].

We used the Enhanced Vegetation Index (EVI) derived from the SAVI index, that was proposed before by Huete [1988], EVI is provided as a standard product calculated from MODIS data on NASA web sites. It was available at 1 km, 500 m and 250 m resolutions starting in February 2000 (Table 1). As SAVI, this index is less sensitive to soil background than the more classical NDVI [Bausch and Neale, 1987; Choudhury et al., 1994; Huete et al., 2002; Huete, 1988] which may be an important property when investigating the spatial variability of f_{cover}, in karst areas where soil is often poorly developed and where rocks outcrop areas can be significant. This is also important when monitoring the evolution of f_{cover} with time when the soil brightness changes, for example because of rain. EVI, as well as SAVI, was also more linearly correlated to f_{cover} than NDVI (Fig. 6) [Carlson and Ripley, 1997; Choudhury et al., 1994; González-Dugo and Mateos, 2008; Olioso et al., 2019; Qi et al., 1994]. Several studies [e.g. Bausch, 1993; Choudhury et al., 1994; Helman et al., 2015] also demonstrated that vegetation indexes less sensitive to soil background, as EVI, presented higher correlations with crop coefficient for ET or for canopy transpiration than NDVI. The relation between f_{cover} and EVI was expressed as:

$$f_{cover} = \frac{EVI - EVI_m}{EVI_x - EVI_m} \quad (10)$$

where EVI_m is the lower EVI value corresponding to bare soil area and EVI_x the maximum EVI value usually corresponding to maximum vegetation cover ($f_{cover} = 1$). The values of parameters EVI_m and EVI_x, specific to MODIS sensors, were set to 0.06 and 0.87 [as derived by Olioso et al., 2019]. Relations between EVI and f_{cover} were also proposed by Mu et al. [2007] with slightly different parameters.

We used EVI data with 250 m and 500 m resolution for the two local forest sites, Puechabon and Font-Blanche, and EVI data with 1 km resolution over the whole Fontaine de Vaucluse watershed (Table 1). 250 m and 500 m data were downloaded using the "point sample" utility from AppEEARS. They corresponded to MODIS collection 5 and to the more recent collection 6. Collection 5 is not anymore available to download today. No significant differences were found between the two collections and the two spatial resolutions when used to feed SimpKcET. Available data correspond to a 16 days synthesis computed from the reflectance acquired every day by MODIS on board of the Terra satellite. The 1 km data were downloaded earlier from the REVERB NASA web site [2016] (this site is now shutdown but a similar tool is available at EARTHDATA, 2019) and corresponded to collection 5 (Table 1). f_{cover} was calculated from EVI provided as 16 days synthesis and then

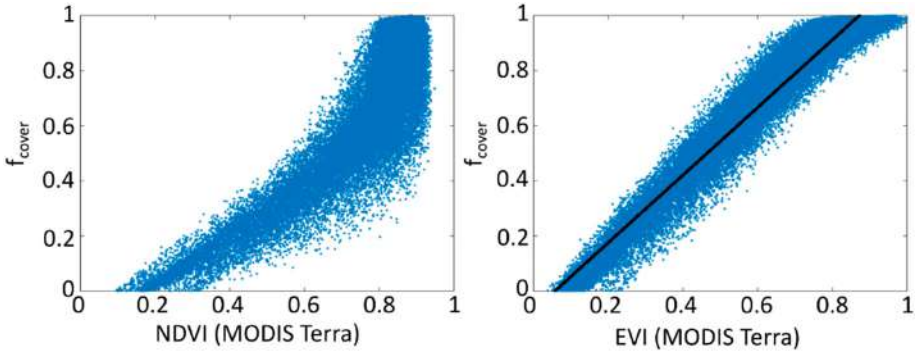

Fig. 6. Relationship between fractional cover and vegetation indices NDVI on the left and EVI on the right. Data were simulated for the MODIS sensor onboard Terra by Olioso et al. [2019] using the PROSAIL model.

interpolated at daily time step using a simple Savitzky-Golay filter (sgolayfilt function in Matlab software choosing a third order polynomial on 51 days moving time windows). This filter also provided a mean for smoothing the time series of f_{cover} by reducing the impact of fast variations of EVI which may be related to "residual cloud contaminations, imperfect atmospheric corrections and directional corrections" [Kandasamy et al., 2013].

In the case of the Avignon agricultural site, MODIS data were not used as the field where ET measurements were performed was too small (2 ha). Instead, we used fraction covers which were computed from Sentinel-2 data with a 20 m resolution thanks to a neural network model. The neural network model was developed at EMMAH and is included in the ESA SNAP toolbox dedicated to the processing of Sentinel satellite images [Weiss and Baret, 2016]. This algorithm has also been integrated in an operational processing chain at University of Natural Resources and Life Sciences of Vienna (Austria) by Vuolo et al. [2016]. For the period we considered, only images from Sentinel-2a were available every 10 days. However, as Avignon was in view of the satellite from two different tracks, data were provided more frequently. Overall, 88 cloud free images were obtained over the simulation period (24 months). As the evolution of Sentinel-2 f_{cover} were quite smooth, a simple linear interpolation was used to provide daily values of f_{cover}.

3.4. SimpKcET implementation

The SimpKcET model was applied using parameters obtained either from the information already available from previous studies over each site or from standard values. In most cases, there was only little information available to set parameter values, so that we used uniform values whatever the soil and the vegetation types. Distributed information was only available for available water capacity of top soil layer ($SAWC_0$) over the Fontaine de Vaucluse watershed [Ollivier et al., 2020]. The maximum value of the canopy transpiration coefficient (k_{Tx}) was set to a uniform value of 0.9 whatever the type of canopy. This value was lower than values usually used for irrigated crops as specified in the FAO56 methods [Allen et al., 1998] that generally ranged between 0.95 and 1.15 (but in some cases up to 1.5). Actually, a lower value was set as the potential ET from SAFRAN data were higher than the FAO56 reference evapotranspiration. A uniform value was applied as no information existed on coefficient variations for the types of vegetation present in our area. No adjustment for vegetation height, albedo, stomata characteristics, wind speed or air moisture was done. Concerning soil parameters, the threshold in the water stress coefficient k_s was considered equal to 2/3 in all situations. Coefficient b in the calculation of k_{ini} was set to 2.5.

Over the whole Fontaine de Vaucluse watershed, the soil water holding capacity SAWC was obtained as a first guess from the $SAWC_0$ map described earlier [Ollivier, 2019; Ollivier et al., 2020]. The water holding capacity for the local sites were taken from previous studies and set to 120 mm, 150 mm and 225 mm for Puechabon [Allard et al., 2008], Font-Blanche [Marie and Simioni, 2014] and Avignon [Garrigues et al., 2015], respectively. For Puechabon and Font-Blanche, these estimations were significantly larger than the estimation of SAWC derived from soil pits which ranged from 40 to 70 mm. Indeed, soil pits measurements are limited by the amount of rocks and the possibility to dig the pits. Tree roots are penetrating through rocks fractures and are able to access underground horizons that are deeper than the one explored through soil pits [Allard et al., 2008; Rambal, 1982]. This behaviour may be exacerbated in dry periods as shown by Carrière et al. [2020a, 2020b] through the analysis of transpired water origin using water isotopes concentration. This may have a large implication on the derivation of the SAWC map over the Fontaine de Vaucluse watershed. Thus, actual available water capacity should be larger than estimated by our previous analysis which only considered soil pits depth. We revised our SAWC map by introducing an additional water quantity termed $SAWC_{add}$ that was directly added to the original SAWC values. Roughly, this can be seen as splitting the reservoir of available water in two parts, $SAWC_0$ which corresponds to the layer accessible to soil pits (and which is equivalent to the original SAWC values as defined by Ollivier et al., 2020) and $SAWC_{add}$ which corresponds to a subsoil layer not accessible to soil pits so that: $SAWC = SAWC_0 + SAWC_{add}$. As no information was available on the spatial variations of this additional subsoil term, a uniform value was used over all the natural and forested areas. Final value of $SAWC_{add}$ was obtained through the calibration of the KaRaMel - SimpKcET model as presented in the next section. No additional value $SAWC_{add}$ was introduced for the agricultural areas, as soil pits were expected to cover the full root zone.

In Puechabon and Font-Blanche, an evaporation reduction coefficient ($1\text{-}f_{rocks}$) of 0.3 and 0.5 was introduced as a very large portion of the soil surface was covered by rocks. These values were derived from the density of rocks and coarse elements given in Allard et al. [2008] and Marie and Simioni [2014]. No reduction was introduced for the crop field in Avignon. No Information on the spatial variations of f_{rocks} was available over the Fontaine de Vaucluse watershed, so that a uniform value was applied over natural and forested areas. As for $SAWC_{add}$ this value was obtained through the calibration of the KaRaMel - SimpKcET model as presented in the next section.

3.5. Model calibration and evaluation

3.5.1. Calibration of KaRaMel

The original KaRaMel model was implemented over the Fontaine de Vaucluse watershed in Ollivier et al. [2020]. Here, KaRaMel was modified to incorporate the SimpKcET model and then tested against Fontaine de Vaucluse discharge and against the original version of KaRaMel with the bucket ET model (Fig. 1). KaRaMel is used to simulate the karst aquifer discharge depending on the ET model. Delaigue et al. [2018] compared the performance of five hydrological model calibration algorithms implemented in R programming language. Their results show that for a simple lumped model calibration, the algorithms differ in the time allocated to find the optimum, but they all converge towards the same optimum. In the present study both a particle swarm optimization [Zambrano-Bigiarini and Rojas, 2013] and differential evolution optimisation [Ardia et al., 2011] algorithms were applied. Both algorithms converged to the same optimum for the initial version of KaRaMel, with five parameters. However, the current version of KaRaMel, including SimpKcET, required the calibration of two additional parameters, which implies a significant additional time of calculation for the particle swarm optimisation algorithm and difficulties to converge. Thus, the calibration step was performed with the differential evolution optimisation, and used a single objective function, the Kling Gupta efficiency (KGE, described in Appendix A) after Gupta et al. [2009]. KGE reached 1 for the best adjustments. Calibration was performed against daily spring discharge of the aquifer from September 2006 to September 2009 (three hydrological years, see Appendix A). The set of parameters providing the best performance with respect to the KGE objective function was retained (it is presented in Appendix A).

3.5.2. Evaluation of evapotranspiration simulations

ET simulated with SimpKcET, on local test sites in Avignon, Puechabon and Font-Blanche were evaluated using the root mean square error (RMSE) and the mean error (bias) against ET measurements (RMSE and bias evaluation functions are given in Appendix A). They were also compared to the ET simulated with the bucket model.

Particular emphasis is placed on the overall form of evapotranspiration. In particular, the influence of the two parameters $SAWC_{add}$ and f_{rocks} on evapotranspiration simulations.

For the Fontaine de Vaucluse test site, the ET simulated with the bucket model is symbolized by ETbu and the ET simulated with SimpKcET by ETsimp. The simulated aquifer discharge depending on ET, is compared to discharge observations using KGE, RMSE and bias.

3.5.3. Cross wavelet analysis

Cross wavelet analysis can be used to provide a representation of the time-scale distribution of correlation between environmental variables [Labat, 2005, Labat, 2010, Sang, 2013, Charlier et al., 2015]. In this study, cross wavelet analysis, including cross wavelet spectrum and wavelet coherence, enables the localization in time-scale space of high degree of relationships between simulated recharge and observed discharge signals. The assumption is that the closer the simulation of the recharge is to reality, the more this signal will be correlated with the observed discharge of the aquifer.

The reader is referred to Kumar and Foufoula-Georgiou [1997], Labat et al. [2000a, 2000b] and Labat [2005] for mathematical details of cross wavelet analysis. Morlet wavelet was chosen as it is fairly well localized in both time and frequency space [Torrence and Compo, 1998], giving good results for the analysis of hydrogeological time series for karst aquifers [Charlier et al., 2015]. Cross wavelet spectrum (XWT) estimates the linear relationship between two signals, revealing the area in the time-scale space with a high common power value. The wavelet coherence (WTC) is a qualitative estimator of the intensity of the correlation of the two series in the time-scale space. The wavelets analysis was performed using the WaveletComp package on R programming language [Rosch and Schmidbauer, 2019].

4. Results

4.1. ET model performances at local scale

The results of the evaluation of the ET model SimpKcET over the three local sites are presented in Fig. 7 and Table 2. Simulated ET are also compared to results obtained from the bucket model that was originally used within KaRaMel.

ET is characterized by a seasonal dynamic in relation to available energy (in particular solar radiation), which particularly drives the climatic demand (ETo), and to vegetation amount and soil water availability which may involve limitation of ET in comparison to ETo. ETo is high during spring and summer. For the three sites, actual ET is low in winter, then increases in spring before decreasing rapidly in early summer. The highest recorded ET from the two forested sites occurs in early summer, when water is still available and vegetation activity and climatic demand are high. The highest ET for the crop site occurs in spring when cereal crops reach their maximum vegetative development. During summer, despite high climatic demand, ET decreases for both the forested sites and the cultivated field. ET from forest areas is limited by the soil's water reserve, which dries up in summer, while crop field ET is limited by plant senescence and then harvesting. After harvest the soil is kept bare or covered by stubbles. In the three sites ET remains low until the first rainy event in early autumn. Then, as water is no longer the main limiting factor, ET dynamics follow the dynamics of climatic demand, which decreases until winter. We can also notice that in winter, ET of the two forest sites are lower than ETo, even with non-limited water availability. This result may be related to the level of vegetation cover, which never exceeded 0.5 and which limits transpiration, and to the presence of coarse elements at the soil surface, which limits evaporation.

The SimpKcET model, which was applied using local value of SAWC and f_{rocks} parameters and standard values for each other parameters, was able to reproduce ET dynamic with a good accuracy. It provided performances with RMSE close to 0.5 mm.d^{-1} and bias lower than 0.15 mm.d^{-1} (Table 2). These performances are good, in particular with no calibration of the model and the use of generic values for parameters such as k_{TX} which may be a very sensitive parameter of SimpKcET. Thus, it is expected that after calibration, performances might be improved further. However, we should notice that the daily ET for these ecosystems is usually low, ranging from 0 to 5 mm.d^{-1}, with an annual average of 1.2 mm.d^{-1}. Periods with the largest differences between the simulated ET and the measurements are most probably linked to the differences between local rainfall and rainfall inputs from the SAFRAN reanalysis (at 8 km resolution). See in particular, the early drop in the simulated ET at the beginning of summer 2009 in Puechabon.

The bucket model poorly reproduced the dynamics of ET, as simulated ETbu is equal to ETo in winter and at the beginning of spring, then decreases down to zero as soon as the soil reservoir is empty. Rainy events refill the soil reservoir and ETbu may then re-increase up to ETo level (or at lower level if precipitation amount is lower than ETo). The simulated ET is nil most of the summer season, with occasional ET peaks after precipitation events. Periods with no ET occur early, when spring is dry as during 2007 and 2008. ETbu retrieves the level of ETo in autumn after the first period of heavy rain.

4.2. Model simulations over the Fontaine de Vaucluse watershed

4.2.1. Influence of SAWCadd and frocks on ET simulated at watershed scale

The two parameters $SAWC_{add}$ and f_{rocks} may have a large impact on the simulation of ET at the watershed scale and thus an impact on the recharge and the flow at the outlet of the karst system. They were calibrated together with KaRaMel parameters by comparing simulated outflow to measurements in Appendix A, giving values of 194 mm for $SAWC_{add}$ and 0.26 for f_{rocks}. In order to illustrate their impact on the simulated ET at the watershed scale, simulations with $SAWC_{add}$ values between 0 and 300 mm and f_{rocks} values between 0 and 100% are presented in Fig. 8.

The value of $SAWC_{add}$ has a great influence on the simulations during the dry period (Fig. 8-a). During that period, the smaller the water retention capacity of the surface and the subsurface, the earlier in the season evapotranspiration is limited. Carrière et al. [2020a, 2020b] show that the water stored in the karst unsaturated zone can have a critical role in the ability of plants to resist water stress periods. $SAWC_{add}$ has no influence on evapotranspiration during the rest of the year, as water availability is higher because of precipitations. The reduction of evaporation by the presence of pebbles at the soil surface (f_{rocks}) has an influence on the evapotranspiration of the watershed throughout the year and in particular for the wet periods (Fig. 8-b). Its influence is minimal during dry periods, as during these periods the transpiration is the main component of the evapotranspiration flux.

4.2.2. ET simulation over the Fontaine de Vaucluse watershed

The daily reference evapotranspiration (ETo) and daily evapotranspiration simulated with SimpKcET (ETsimp) and the bucket model (ETbu) at the scale of the Fontaine de Vaucluse watershed are presented in Fig. 9. Over the validation period from September 2009 to May 2015, ETo ranged from 0.03 to 8.7 mm.d^{-1}, ETsimp from 0.02 to 4.8 mm.d^{-1} and ETbu from 0 to 7.5 mm.d^{-1}. The general ET dynamics were quite similar from one year to another and were very coherent with the dynamics obtained at the local sites. The climatic demand presented a very marked seasonal cycle, increasing from winter to summer and decreasing from summer to winter. Simulated ET were lower than ETo during spring and summer indicating the impact of the depletion of available water. Similarly, to local forest sites, ETsimp is always lower than ETo in winter, because of the reduction of soil evaporation imposed by the f_{rocks} parameter which was set to 0.26 and the reduction of transpiration imposed by low values of f_{cover} in winter (in particular for deciduous forest and crops).

At watershed scale, differences between the two ET models were similar to those observed at local scale. The ETbu simulated by the bucket model sustained the climatic demand as long as water was available and stopped when the soil reservoir was empty, while SimpKcET exhibited slower decreases in ET without reaching zero. The bucket model reached the nil ET level in summer, but later than for the simulations at local sites (and never in spring). This is explained by lower ETo, higher rain and by the spatial distribution of ET responses related to

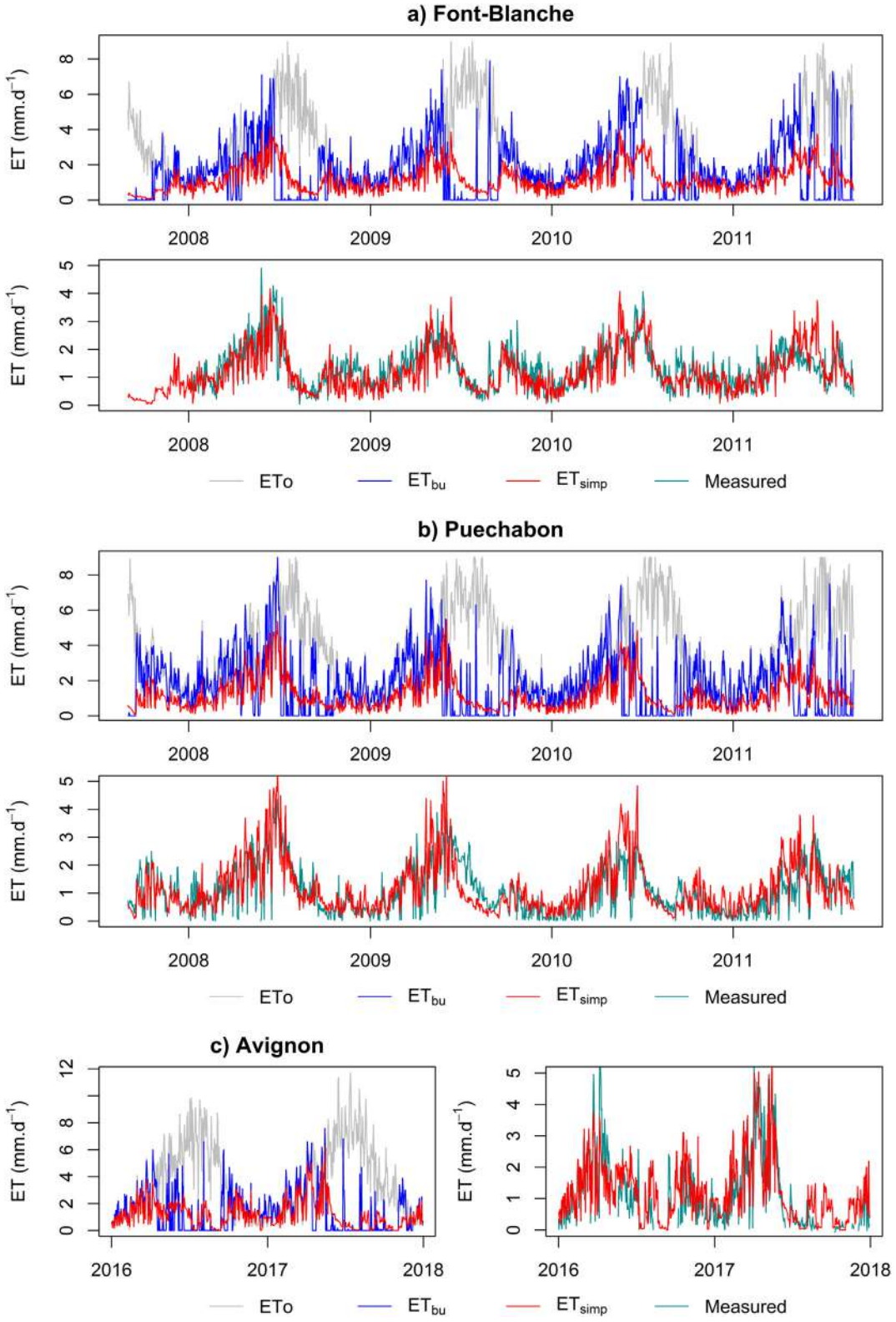

Fig. 7. Reference evapotranspiration (ETo, grey lines), simulated evapotranspiration with the bucket model (ETbu, blue lines) and SimpKcET (ETsimp, red lines) and measured evapotranspiration (Measured, green lines) from September 2007 to August 2011 for Font-Blanche and Puechabon sites and from January 2016 to December 2017 in Avignon. (For interpretation of the references to colour in this figure legend, the reader is referred to the web version of this article.)

spatial variations in SAWC and f_{cover} which combine together for generating ET at the watershed scale.

Examples of ET simulated for different types of land cover are given in Fig. 10, together with the evolutions of f_{cover}, k_T, k_E and k_S for year 2010. Forests of deciduous oaks, evergreen oaks, pines and beeches and an agricultural area are presented. We selected model meshes areas with values of $SAWC_0$ close to 110 mm. Aerial photographs from the Region Provence-Alpes-Côte-d'Azur survey of the selected areas are presented in Appendix C showing the diversity in vegetation conditions. The activity of beech forests and deciduous oak forests had strong

Table 2
parameters and results for the SimpKcET model for the three test sites with evapotranspiration measurements. The RMSE and bias indices (described in Appendix A) are evaluated at daily and monthly time scales against evapotranspiration measurements performed using micrometeorological tower stations.

	Model parameters				Model performances			
					Daily scale [mm.d^{-1}]		Monthly scale [mm.month^{-1}]	
	SAWC [mm]	k_{TX}	f_{rocks}	b	RMSE	bias	RMSE	bias
Font-Blanche	150	0.9	0.5	2.5	0.49	0.14	8.63	4.36
Puechabon	120	0.9	0.8	2.5	0.50	−0.04	10.6	−1.85
Avignon	200	0.9	0	2.5	0.51	0.13	–	–

seasonal dynamics with a maximum fraction cover up to 0.6 for deciduous oak and 0.8 for beech at the end of spring and between 0 and 0.2 in winter. Evergreen oak forest and pine forest had lower seasonal changes with fraction covers between 0.2 and 0.4. The agricultural area had also a low fraction cover (between 0 and 0.4) with a multimodal seasonal dynamic related to the mixture of various types of crops with different vegetation cycles (mostly wheat, lavender and grassland). When considering simulated ET, the global dynamics were very similar for the different land cover, with some slight variations related to the differences in f_{cover} and the dynamics of water stress related to SAWC.

The examination of k_T, k_E and k_S provide insights in the regulation of evapotranspiration for each vegetation type (Fig. 10). Soil evaporation is strong during autumn and winter, it decreases in spring to reach values close to zero in summer, in relation to higher climatic demand and lower occurrence of rainfall. The highest vegetation fraction covers (e.g. for the beech forest) also tend to limit soil evaporation.

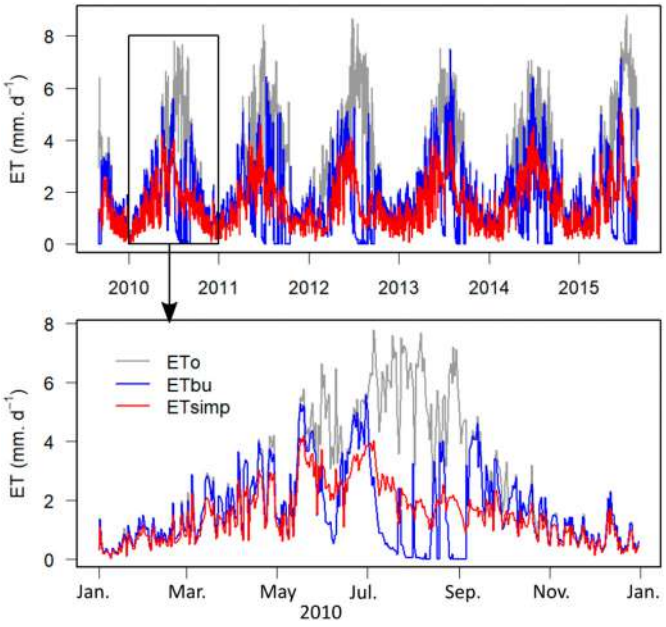

Fig. 9. Reference evapotranspiration (ETo), evapotranspiration simulated with the bucket model (ETbu) and evapotranspiration simulated with SimpKcET (ETsimp) for watershed of Fontaine de Vaucluse aquifer.

Transpiration strongly depends on f_{cover} in winter and autumn and on the deficit in available water by mid-spring and summer (see k_S).

Spatial variations of ET calculated with SimpKcET are presented in Fig. 11 at monthly time scale for year 2010. The spatial pattern of ET is

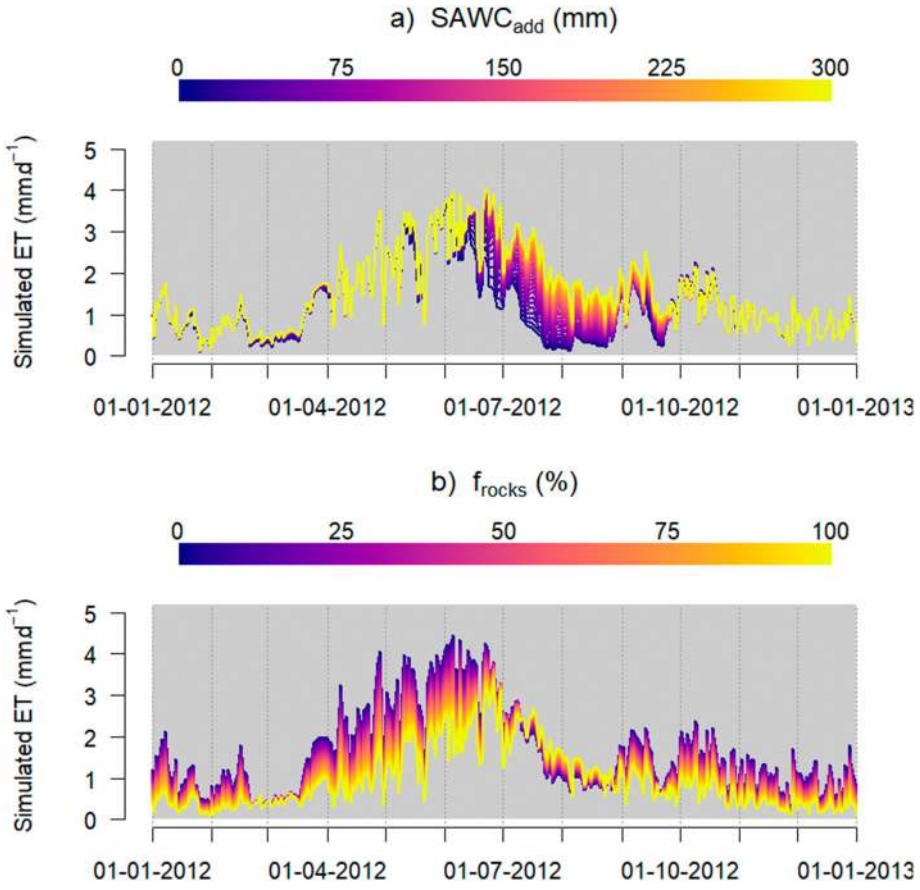

Fig. 8. At the scale of the Fontaine de Vaucluse watershed, the ET simulation is sensitive to the values of the parameters: a) $SAWC_{add}$ and b) f_{rocks}.

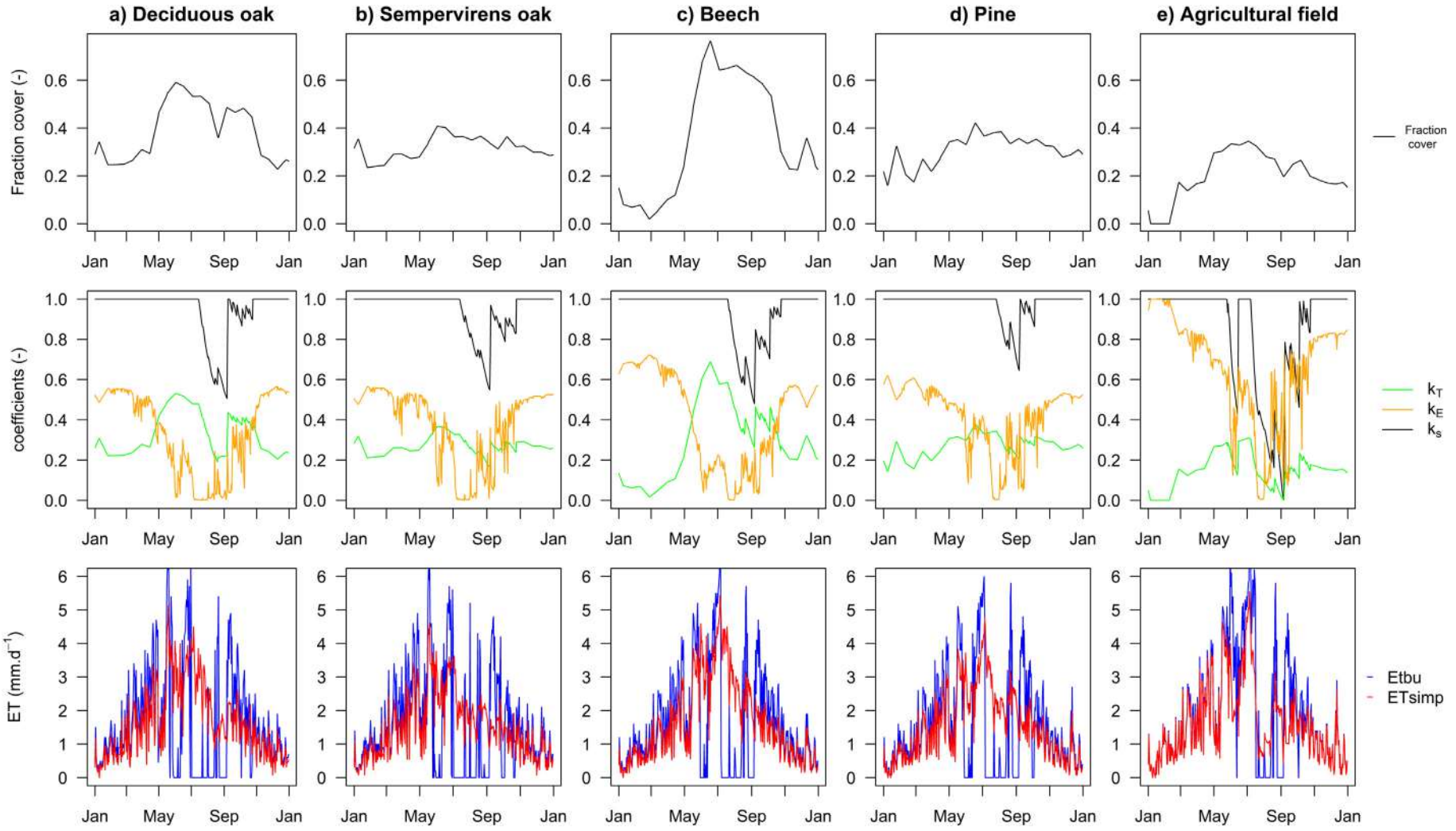

Fig. 10. The vegetation fraction cover (f_{cover}), the soil evaporation coefficient (k_E), the water stress coefficient (k_S) and the canopy transpiration coefficient (k_T) depending on the vegetation of area of Fontaine de Vaucluse watershed: a) Deciduous oak, b) Evergreen oak, c) Beech, d) Pine and e) Agricultural field during 2010.

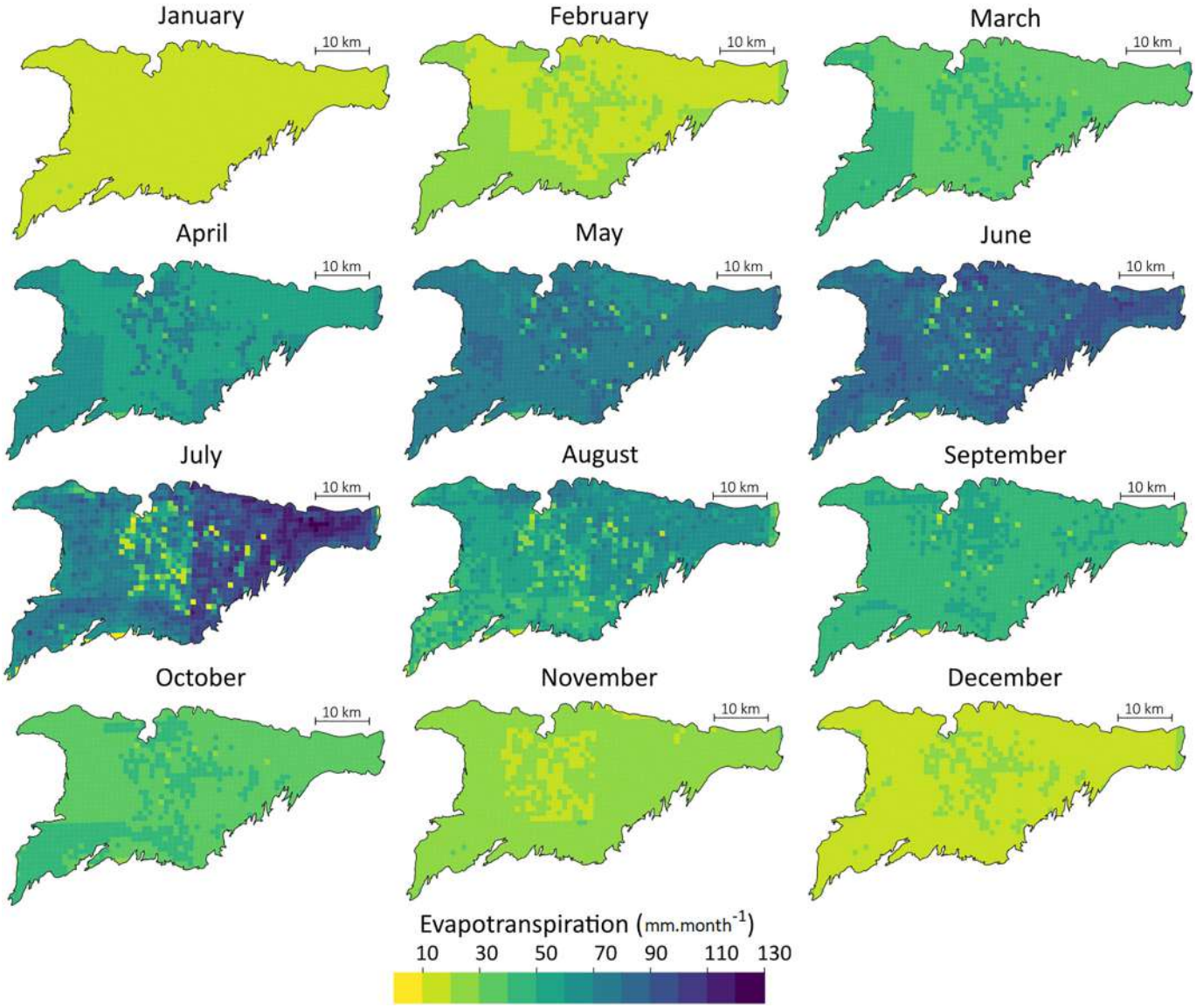

Fig. 11. Spatial distribution of monthly evapotranspiration over Fontaine de Vaucluse watershed during 2010.

strongly controlled by the pattern of precipitation. The 8 by 8 km grid of the SAFRAN meteorological dataset is clearly visible, as well as a larger scale pattern which is related to the definition of "isoclimatic" zones (SYMPOSIUM zones) for distributing meteorological information at the scale of the SAFRAN grid by METEO-FRANCE (for more details see the Appendix C in Ollivier, 2019). This larger scale pattern is clearly visible in July, the values are contrasted between the East and West of the watershed, in reason of one strong precipitation event mainly affecting the East part of the watershed at mid-June (West: ~50 mm; East ~150 mm).

At a finer scale than SAFRAN grid, the spatial pattern of evapotranspiration is controlled by the pattern of $SAWC_0$ and f_{cover}. The role of the soil is stronger where $SAWC_0$ is low. Areas with low $SAWC_0$ are also flat areas with a high density of karst features (dolines and faults) which promote recharge and reduce the availability of water for evapotranspiration (see geological map in Ollivier et al., 2020). The patterns of meteorological data and SAWC explain most of the spatial variability of the monthly evaporation from October to April. From May to September, the spatial variability of the evapotranspiration is also impacted by the vegetation activity.

4.2.3. Evaluation of the karst response (discharge)

Both versions of the model (KaRaMel + bucket model and KaRaMel + SimpKcET) were calibrated against flow measured at the Fontaine de Vaucluse spring over the 2006–2009 period (see Appendix A). The models were evaluated over the 2009–2015 period. According to the

Table 3
The KaRaMel's performance over the validation period (2009–2015), according to the used evapotranspiration model.

	All data from 2009 to 2015			Low flows ≤8 $m^3.s^{-1}$	Int. flows [8,23] $m^3.s^{-1}$	High flows ≥23 $m^3.s^{-1}$
	KGE	bias	RMSE	RMSE		
KaRaMel+ Bucket	0.92	−0.11	4.59	1.96	3.69	7.21
KaRaMel+ SimpKcET	0.95	0.08	3.41	1.02	2.81	5.40

statistical analysis of daily flow, daily flows above the 3rd quantile (> 23 $m^3.s^{-1}$) correspond to high water periods, while flows below the 1st quantile (< 8$m^3.s^{-1}$) correspond to low water periods. The introduction of a better representation of the ET induces an improvement of the simulation of the aquifer flows, as summarized by the increase of the KGE from 0.92 to 0.95. In addition, the average error between the simulation of the aquifer flows and the observation decreases from 4.6 to 3.4 $m^3.s^{-1}$. These reductions concerned the high water and low water, since the mean error decreased by about 25% and 50% respectively (Table 3). This is illustrated, for example, by a better estimation of the flood flow observed in winter 2011 and spring 2012 (Fig. 12).

Monthly variabilities of ET, recharges and discharges of the hydrosystem were linked to the type of evapotranspiration model (Fig. 12). The evapotranspiration simulated with SimpKcET (ETsimp) was usually slightly lower than the evapotranspiration simulated with the bucket (ETbu) model in autumn, winter and spring. On the contrary, ETsimp was higher than ETbu from late spring to late summer. This difference in evapotranspiration dynamics induced differences in the hydrosystem's recharge volumes. Winter and spring refills were slightly higher with KaRaMel + SimpKcET and provided greater support for the hydrosystem's low water levels in summer (Appendix B). However, the hydrosystem was mostly recharged in winter and spring, whatever the evapotranspiration model used. In summer the recharge rate was close to zero and recharge only occurs during high intensity rainfall events. Recharge became significant again at the beginning of fall when the first major rainfall events occurred. At that time the simulated recharge was significantly lower with SimpKcET than with the bucket model. Conversely, SimpKcET simulated higher recharge events during the following months till spring. These changes in simulated recharge time dynamics directly impacted the simulated discharge which was decreased in autumn and winter and increased in spring when using SimpKcET. The resulting dynamic of simulated discharge was significantly improved with SimpKcET.

4.2.4. Recharge and discharge relationship

Cross wavelet spectrum (XWT) and cross wavelet coherence (WTC) analysis are used to highlight the relationships between simulated recharge and observed discharge (Qobs) signals (Fig. 13). The recharge is simulated with the KaRaMel model using the bucket model (Rbu) or the SimpKcET model (Rsimp). On the cross-wavelet spectrum (XWT), the y-axis represents the frequencies expressed in periods (in days) and the x-axis the time. The colour bars represent the value of the wavelet coefficient with low to high powers (from blue to red). These analyses enable to identify whether the use of the SimpKcET model in a karst hydrological model provides more coherence between the hydrosystem's input and output signals compared to the use of the bucket model.

The XWT between Rbu and Qobs or Rsimp and Qobs have similar patterns (Fig. 13-a, b). For periods of 2 to 64 days (y-axis), times without linear relationships alternate with times of strong linear relationships between recharge and discharge. This corresponds to the seasonality of the recharge, during the wet season, the causal link between recharge and discharge is linear, while during the dry season the link is almost non-existent since recharge is low or nil. Comparison of the cross-wavelet coherence analyses (WTC) proves that the correlation is more intense with Rsimp than with Rbu (Fig. 13-c, d). The calculation of the mean coherence by period reveals that the use of SimpKcET model brings improvements for mid-term components with periods greater than 100 days (> 3 months). It is also true for shorter periods, as for recharge events of year 2012 delimited by the white rectangle in Fig. 13. Year 2012 was particularly dry but two important recharge events occurred in May. The first event happened from April 28th to May 4th

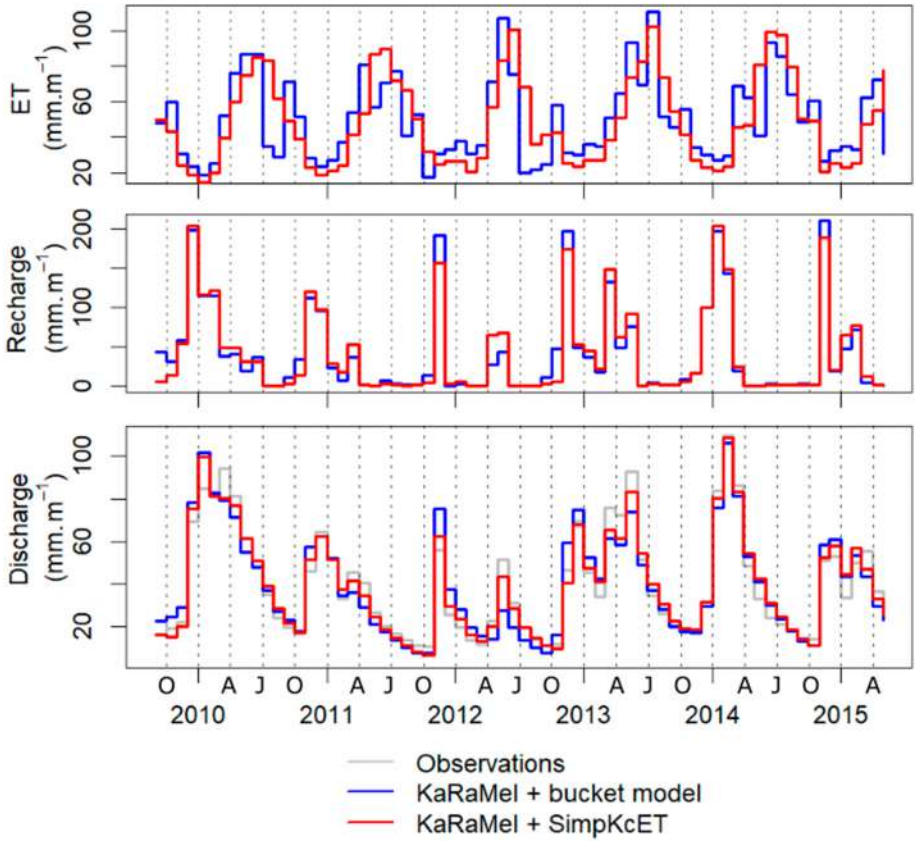

Fig. 12. Monthly time series of evapotranspiration, recharge and outlet discharge of Fontaine de Vaucluse aquifer depending on the evapotranspiration model (bucket or SimpKcET). O: October, A: April, J: July.

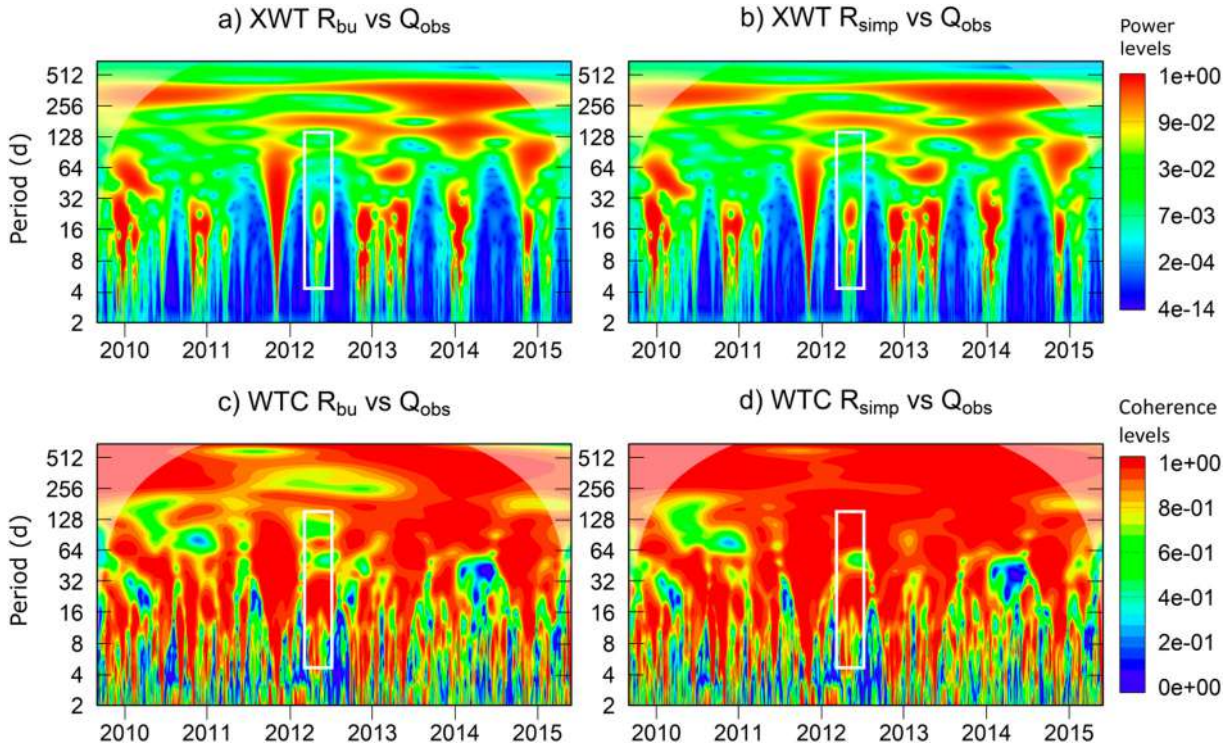

Fig. 13. Cross wavelet analysis between modelled recharge signals (either Rbu or Rsimp depending on the evapotranspiration model) and discharge measures of the outlet of the aquifer (Qobs). a) and b) Cross wavelet spectrum (XWT), c) and d) cross wavelet coherence spectrum (WTC). The white rectangle delimits an area where both the linear relationship and the intensity of this relationship are stronger with Rsimp than with Ru.

with 35 mm of recharge. The second event happened from the 20th to the 24th of May with 25 mm of recharge. Cross wavelet analysis highlighted a better correlation between discharge observations with Rsimp than with Rbu (Fig. 13-a, b). Moreover, this relationship is more intense with Rsimp (Fig. 13-c, d).

Previous results have shown that Rsimp seems more realistic in quantitative terms, and shifts the start of recharge times by a few weeks. Wavelet analysis adds that the simulated recharge is more correlated with the observed discharge when it is simulated with the SimpKcET model. However, the seasonal dynamics of recharge remain globally the same since it is imposed by the rainfall regime and the aquifer has no exchange with neighbouring aquifers.

5. Discussions

Mediterranean karst landscapes are characterized by diverse land uses with agricultural areas and areas of wild vegetation. The vegetation is formed by forests with a diversity of tree species, which are well-adapted to periodic water stress. The soils are often poorly developed and rich in stones. The SimpKcET model was developed to introduce a realistic description that accounts of the main evapotranspiration processes in karst hydrological modelling under Mediterranean climate. The need to integrate a more realistic evapotranspiration model for the evaluation of underground reserves in karst regions was also raised by Jódar et al. [2018] and Sarrazin et al. [2018]. The evapotranspiration models they proposed are more complex and require more parameters describing soil water transfer and retention (much more in the model of Sarrazin et al., 2018). Most of vegetation parameters may be approximated after data recorded by vegetation ecophysiological monitoring [Lin et al., 2015] or calibrated after evapotranspiration measurement [as provided by FLUXNET network, Baldocchi et al., 2001, Chu et al., 2017], even if strong assumptions must be made for mixed forests and land cover. However, most of the uncertainties in their models are due to soil properties that remain challenging to estimate because they are highly variable at a short scale. The sensitivity analysis conducted by Sarrazin et al. [2018] shows that the first uncertainty factor in recharge estimation is the spatial variability factor of soil properties, followed by soil properties. The results of the sensitivity analysis led by Garrigues et al. [2015] demonstrate that the uncertainty of the spatial and temporal variability of evapotranspiration from cultivated land is mainly due to soil properties. Ollivier et al. [2020] observes that the distribution of the SAWC has a strong influence on the discharge modelling of the Fontaine de Vaucluse hydrosystem. We assume that the estimation of evapotranspiration is more appropriate with a conceptual model than with a physical model as long as the properties of the soil cannot be known at any point in space.

In a first step, the SimpKcET model was evaluated against evapotranspiration records of three sites with different land cover: agricultural field, mixed forest of oak and pine, and oak forest, located southeast of France under a Mediterranean climate. The daily evapotranspiration simulated with SimpKcET were of good quality with an RMSE of about 0.5 mm.d^{-1} at ET measurement sites without calibration. In a second step, the SimpKcET model was implemented into the Karst Recharge and Discharge Model (KaRaMel) in order to evaluate the impact of evapotranspiration distribution on the discharge of the karst aquifer of Fontaine de Vaucluse. The original KaRaMel was using the bucket model to evaluate the evapotranspiration [Ollivier et al., 2020].

The evapotranspiration simulated with SimpKcET is significantly lower than climate demand (ETo, estimated using the Penman-Monteith equation). This contrasts with the simulated evapotranspiration with the bucket model, which was equal to ETo as long as there are water reserves in the soil, and soil water is readily consumed. SimpKcET has made it possible to simulate the regulation of evapotranspiration, which is particularly important during the hottest season. In the Mediterranean climate, climatic demand and plant activity are high in summer but water scarcity limits both transpiration and evaporation. This drastic limitation of evapotranspiration is correctly simulated by SimpKcET for local sites and for the studied watershed. The underground regulation of evapotranspiration, through the calculation of k_s, allows a more realistic simulation of the evolution of soil water,

which is stored longer during the dry season than with the bucket model.

A specificity of SimpKcET lies in the introduction of the impact of the surface fraction of coarse elements on evaporation through the f_{rocks} parameter. Indeed, karst superficial zones are often dominated by areas with large proportions of coarse elements and/or denuded carbonate rocks that limit soil surface evaporation. We showed that the impact of the f_{rocks} parameter is high except during the dry period and that it is responsible for reducing significantly soil evaporation, in particular over the two local forest sites. In consequence, f_{rocks} has also a significant impact on the aquifer recharge. Thanks to the inclusion of the f_{rocks} parameter, SimpKcET is well adapted to the simulation of evapotranspiration over Karst systems that have poorly developed soils and a limited amount of soil evaporation compared to transpiration.

Given the limited available data to describe soil and vegetation at large scale, the proposed SimpKcET uses few parameters easily implemented for all types of landscape. Moreover, some parameters, as $K_{c,max}$ and b, were given constant values over the watershed as no real reference values existed for the different ecosystems and soils. These values were providing good results over different ecosystems at local sites (wheat in Avignon, holm oaks in Puechabon and mixed holm oaks and aleppo pines in FontBlanche) and were the used at the watershed level.

We observed differences between $SAWC_0$ derived from soil pits analysis and SAWC values derived in previous local studies for the two forests in Puechabon and Font-Blanche. The $SAWC_0$ values obtained from soil pits in the vicinity of the Font-Blanche and Puechabon sites are respectively in the range of 40 to 80 mm and 30 to 70 mm, while the local values from earlier studies are 145–170 mm (Marie and Simioni, 2014; Simioni et al., 2016) and 120 mm (Allard et al., 2008). Soils are very rich in coarse elements and the carbonate bedrock is very close to the surface which limits the depth of investigation of the soil pits that are usually dug by manual force. In a similar environment, Rambal et al. [2003] and Rambal [1984] showed that the deep roots of holm oak and kermes oak (a close relative of holm oak) allow them to exploit water in the sub-soil at least up to 4.5 m, with an accessible water reserve between 300 and 450 mm. Nourtier et al. [2014] showed that silver firs in the northern part of the Ventoux mountain were withdrawing water as deep as 4 m and possibly further in some part of the area. Carrière et al. [2020a] has proved by isotopic monitoring that during dry summers, a noticeable part of the water consumed by the trees comes from deep reservoir underground.

The SAWC deduced from the soil pits of natural areas therefore does not allow the assessment of the amount of water available for plant transpiration deeper in the sub-soil. In addition, several studies also showed the presence of perennial water stocks in the unsaturated karst zone [e.g. Carrière et al., 2016; Pronk et al., 2009; Watlet et al., 2018]. As there is no data available for distributing the sub-soil waters, potentially exploited by plants, the same value has been assigned to all areas covered by natural ecosystems (forests, pastures). While cropped area were mainly present over well-developed soil. Valley bottom, flat areas or zones with significant karstic weathering that favour the accumulation of decalcification clays and other sediments resulting from erosion. The sub-soil water available for plants, the proportion of coarse elements and rocks at the soil surface were calibrated at catchment scale to 194 mm and 26% respectively. When compared to the total SAWC in Puechabon or FontBlanche, this SAWCadd value looks high. However, 200 mm would correspond to a water holding capacity of 5% for 4 m layer which is in agreement with values observed in other karst systems in South of France as Rambal [1984]. It is difficult to evaluate the fraction of rocks over the watershed as this fraction varies strongly from place to place, between 0 and 100%. However, with large areas having high frocks, see for instance aerial photography of Appendix C.

At the moment, it is only possible to provide overall values of SAWCadd and frocks that were obtained through model calibration. This seems to be the wisest solution as long as soil properties are not mapped, which may be different in the future, as the international community is working to improve soil property maps in particular based on satellite information (see Arrouays et al., 2017 for example). It is likely that a better spatial distribution of soil properties would improve the realism of simulated evapotranspiration. Sensitivity studies of evapotranspiration models show the preponderance of simulation sensitivity to soil parameters [Garrigues et al., 2015; Sarrazin et al., 2018] and the hydrological model KaRaMel is also sensitive to the distribution of SAWC [Ollivier et al., 2020]. However, it is also likely that the low spatial resolution of climate data masks some of the spatial heterogeneity of evapotranspiration. Here, we used the SAFRAN data from METEO-FRANCE which are distributed on an 8 km by 8 km grid. This is the best spatial resolution available at the moment in France over long periods of time, but it may be not fine enough to resolve the spatial variability related to topography over our area. However, resolution may improve in the future with the increasing resolution of atmospheric models and the use of precipitation products derived from meteorological radar measurements.

Since the use of SimpKcET allows a more realistic simulation of watershed evapotranspiration, we expect that simulated hydrosystem flows, such as recharge, can also be more realistic. We have demonstrated the consistency between the simulated recharge and the observed discharge at the seasonal, annual and multi-year scales. The use of evapotranspiration with realistic daily, weekly and seasonal behaviours improves the modelling of daily recharge and discharge of the Fontaine de Vaucluse aquifer. The Fontaine de Vaucluse aquifer has the following characteristics: karstic features are numerous (e.g. dolines, lapiaz), the karst network is well developed, land use is mainly sparse forest, moors, scrubland, planted forests and agricultural areas, and the impluvium is located under a Mediterranean climate. Such characteristics are shared by many aquifers around the Mediterranean [Ford and Williams, 2007]. The recharge and flow of the Fontaine de Vaucluse aquifer are responsive to seasonal cycles and to the spatial distribution of evapotranspiration. This is certainly the case for all hydrosystems that have similar characteristics. Thus, the application of a model as SimpKcET might benefit to improve the simulation of the flows within those other aquifers.

The SimpKcET model uses a conceptual representation of evaporation and transpiration processes which require a lower amount of information. The use of vegetation indices to constrain the fraction cover (f_{cover}) makes it possible to avoid an exhaustive knowledge of the vegetation in place, and provide a better consideration of mixed cover. The vegetation indices (EVI) used have a coarser spatial resolution than those used by Jódar et al. [2018], but its temporal resolution is finer, allowing a better representation of the temporal dynamics of transpiration. Estimation of fraction cover from remote sensing data could be based on different algorithms (neural network, relation to vegetation indices…) and/or different satellite data (MODIS, VEGETATION/PROBA-V) that may affect the estimation of Kc [Gao et al., 2020]. Spectral properties of specific vegetation type can also affect the relation between vegetation indices and fcover [Carpintero et al., 2018]. Both these effects that could affect the estimation of ET were not investigated in our study which in a first step provided satisfactory results. Analysis of how changes in f_{cover} derivation can impact the derivation of ET using SimpKcET will be performed in further works. For example, we will investigate the possibility to derive K_c from f_{cover} as obtained from the COPERNICUS Land Monitoring Service [COPERNICUS Land Monitoring Service, 2020] as this service directly provide f_{cover} on a real time basis. However, it may provide different values of f_{cover} compared to the values we derived in our work as involved algorithm are very different Copernicus product is based on a neural network trained on a large dataset of ground data, see Baret et al. [2013].

6. Conclusions

We proposed an evapotranspiration model that enables a consistent representation of main processes (vegetation transpiration and soil

evaporation), with available parameters for all types of vegetation. The model consistency was evaluated against the most commonly used model into hydrological models of karst hydrosystem.

The SimpKcET model is based on the description of the soil's water retention capacity and the use of the fraction of vegetation cover to simulate plant transpiration and soil evaporation. The use of remote sensing data, in particular the Enhanced Vegetation Index (EVI), enables an exhaustive description of daily variation of vegetation development and its impact on evapotranspiration. The description of the soil reservoir is simple with only the soil available water capacity and the fraction of rocks of soil surface to determine, after ecological knowledge or soil pits observation, or to calibrate. Thanks to the inclusion of the frocks parameter that limits soil evaporation, the model is well adapted to the description of evaporation over karst systems.

SimpKcET was evaluated favourably against flux tower data on local sites in a first step and spring discharge of a large karst aquifer in a second step, showing that it enables the simulation of spatial and temporal variation of the evapotranspiration. Our results show the proximity between the daily estimates and the daily observations of evapotranspiration for forested and cultural field cover under a Mediterranean climate.

SimpKcET is applied at watershed scale under a Mediterranean climate (the karst aquifer of Fontaine de Vaucluse). It is an ideal test site with a wide range of land cover and landscape. The consideration of spatial and temporal distributions of soil evaporation and plant transpiration has an impact on recharge distribution, thus on the karst system answer. The use of SimpKcET model enables a more realistic estimation of the evapotranspiration and of the aquifer discharge, thus it is assumed that the simulated spatial and temporal recharge of the hydrosystem is also realistic. This is confirmed by the wavelet analysis of the recharge-discharge relationship. The use of a realistic evapotranspiration induced more coherence between the simulated recharge and observed discharge at seasonal, year and multi-year scales. This experiment validates the use of the vegetation index from remote sensing data to estimate the evapotranspiration of a large watershed with various land cover.

Different methods are available, but, at the moment, compared to the standard “working methods” in hydrogeology, the inclusion of remote sensed ET is “costly” (time, data handling, knowledge) [Jódar et al., 2018]. In a context of global changes, it is very important now to provide operational ET products to users with a quantification of uncertainties and adapted to the relevant time scales and spatial scales. The SimpKcET is robust for various land cover and can be easily implemented into hydrological models. This may improve the determination of effective aquifer recharge and in particular its time dynamics, as well as its spatial variability. The joint use of KaRaMel and SimpKcET allows a realistic simulation of the spatial and temporal distribution of the system's recharge. This will help groundwater managers to better estimate the rate of renewal of the resource. An accurate estimate of the influence of surface properties (vegetation, land use, soil) is important in order to anticipate the impact of global changes on groundwater resources.

CRediT authorship contribution statement

Chloé Ollivier: Conceptualization, Methodology, Software, Writing – review & editing. **Albert Olioso:** Conceptualization, Methodology, Software, Writing – review & editing, Project administration, Funding acquisition. **Simon Damien Carrière:** Conceptualization, Methodology, Writing – review & editing. **Gilles Boulet:** Methodology. **Konstantinos Chalikakis:** Project administration, Funding acquisition. **André Chanzy:** Investigation, Data curation, Resources. **Jean-Baptiste Charlier:** Methodology. **David Combemale:** Investigation, Data curation, Resources. **Hendrik Davi:** Investigation, Data curation, Resources. **Christophe Emblanch:** Project administration, Funding acquisition. **Olivier Marloie:** Investigation, Data curation, Resources. **Nicolas Martin-StPaul:** Investigation, Data curation, Resources. **Naomi Mazzilli:** Methodology. **Guillaume Simioni:** Investigation, Data curation, Resources. **Marie Weiss:** Investigation, Data curation, Resources.

Declaration of competing interest

The authors declare that they have no known competing financial interests or personal relationships that could have appeared to influence the work reported in this paper.

Acknowledgements

This work used eddy covariance data acquired and shared by the FLUXNET community, including these networks: AmeriFlux, AfriFlux, AsiaFlux, CarboAfrica, CarboEuropeIP, CarboItaly, CarboMont, ChinaFlux, Fluxnet-Canada, GreenGrass, ICOS, KoFlux, LBA, NECC, OzFlux-TERN, TCOS-Siberia, and USCCC. The ERA-Interim reanalysis data are provided by ECMWF and processed by LSCE. The FLUXNET eddy covariance data processing and harmonization was carried out by the European Fluxes Database Cluster, AmeriFlux Management Project, and Fluxdata project of FLUXNET, with the support of CDIAC and ICOS Ecosystem Thematic Center, and the OzFlux, ChinaFlux and AsiaFlux offices.

We thank the investigators of the evapotranspiration monitoring sites for allowing us to use their data, and in particular Jean-Marc Ourcival (Puechabon).

The authors greatly thank Fred Baret for advices about the estimation of fraction cover from remote sensing data. The SAFRAN data were provided by METEO-FRANCE, and EVI data by NASA, we appreciate the support from Cécile Velluet and Fréderic Huard (INRAE).

This work benefited from fruitful discussion within the KARST observatory network (SNO KARST) initiative from the INSU/CNRS. SNO KARST aims to strengthen knowledge sharing and to promote cross-disciplinary research on karst systems at the national scale.

Financial support for part of the study was provided by CNES APR (PITEAS project) related to evapotranspiration estimation from remote sensing data. Financial support for a part of the study was provided from JPI WaterWorks2017, the project FLUXMED is gratefully ackowledged.

Appendix A. Setting of hydrological model

A.1. KaRaMel model

KaRaMel is a hydrological model of karst. Karst hydrosystems are too heterogeneous for a distributed model to be used, so the assumption was to distribute only the most important processes. The distribution of the parameters is deduced with readily available spatial data such as geology, land use, soil characteristics, presence of karstic forms.

The aquifer is gridded in square cells. The same lumped structure is used to represent the flows and water stocks that occur in each cell. There are no water exchanges between cells. The first reservoir represents the soil and subsoil, it receives precipitation and irrigation, enables evapotranspiration and infiltration to deeper reservoirs. The infiltration feeds two deep reservoirs acting for a slow and fast water transfer that occurs in the aquifer. The sum of the discharge from cells represents the aquifer discharge.

The KaRaMel and its setting for the Fontaine de Vaucluse aquifer are described in detail by Ollivier [2019] and Ollivier et al. [2020]. When applied to the Fontaine de Vaucluse watershed 1550 cells are used to represent the 1160 km^2 area (most of the cells having a surface about 1 km^2).

A.2. KaRaMel and SimpKcET parameters

The first version of KaRaMel applied on the Fontaine de Vaucluse aquifer relies on 5 parameters:

- The coefficient x partitions the infiltration between slow and fast flows; the distribution of x depends on the intrinsic vulnerability indices. The intrinsic vulnerability of the watershed can be low (x_L) or high (x_H).
- kc and km are the specific discharge coefficients of reservoirs that control fast flows and slows flow respectively; the distribution of kc depends on the intrinsic vulnerability indices. The intrinsic vulnerability of the watershed can be low (kc_L) or high (kc_H).

The water holding capacity of the first reservoir of KaRaMel was set equal to the soil available water capacity, explored by soil pit. The implementation of SimpKcET into KaRaMel brings implies the calibration of SimpKcET parameters:
- $SAWC_{add}$ stands for the water holding capacity of subsoils exploited by plant roots (which can not be measured in soil pits)
- frocks is the fraction of rocks that cover the soil surface.

Both parameters concerned all surfaces with the exception of crop fields for which we can assume a low level of coarse elements near the soil surface and that soil pits cover the full depth of the soil.

A.3. Calibration and validation of the model

Model parameters were initialized with a three-year period (2003-2006), this prevents simulation bias induced by the initialization of the parameters. Model's parameters are calibrated (Table A.3-2) over a three years period, from September 2006 to august 2009. These three years represent a large panel of hydric situations, Table A.3-1. The daily observed discharge sequence from September 2009 to May 2015 is compared with discharge simulation to validate simulation.

Table A.3-1
Statistical description of daily discharge time series au Fontaine de Vaucluse, depending modelling periods: warm-up (2003–2006), calibration (2006–2009) and validation (2009–2015).

Fontaine de Vaucluse daily discharge [$m^3.s^{-1}$]						
Periods	Min	1st quantil	Median	Mean	3rd quantil	Max
2003–2006	4.3	6.8	9.7	13.3	16.4	82.5
2006–2009	2.8	6.7	9.1	13.6	17.8	60.6
2009–2015	3.9	7.9	14.0	17.5	23.5	63.0
2003–2015	2.8	7.0	9.7	13.2	16.4	82.5

The calibration is performed with the differential evolution optimisation algorithm [Ardia et al., 2011], with a unique objective function, the Kling-Gupta efficiency (KGE). Model performances are evaluated with two additional functions, the root mean square error (RMSE) and the bias.
The KGE function images the Euclidian distance from the ideal point in the scaled space of three components (r, β and α). r is the linear correlation coefficient between measurements and simulated flows, β the ratio between mean simulated flow and mean observed flow and α the ratio between standard deviation of simulated values and standard deviation of observed values. The KGE reaches 1 for the best adjustments.

$$KGE = 1-\sqrt{(r-1)^2+(\alpha-1)^2+(\beta-1)^2} \quad (A.1)$$

The simulated ET is evaluated using the root mean square error (RMSE) and the mean error (bias) against ET measurements.

$$RMSE = \sqrt{\frac{1}{n}\sum (v_o-v_s)^2} \quad (A.2)$$

$$bias = \frac{1}{n}\sum (v_o-v_s) \quad (A.3)$$

where n is the number of simulated time steps, v_o the observed variable and v_s the simulated variable.

Table A.3-2
Calibrated values of KaRaMel's parameter.

	x_L	x_H	km	kc_L	kc_H	$SAWC_{add}$	f_{rocks}
KaRaMel with bucket ET model [Ollivier et al., 2020]	0.90	0.66	0.0094	0.23	0.14	–	–
KaRaMel with SimpKcET	0.97	0.65	0.009	0.14	0.78	194	0.26

Appendix B. Fontaine de Vaucluse discharge simulations

In the present study, the Karamel model is applied to the karstic aquifer of the Fontaine de Vaucluse. This enables the simulation of the discharge of the Fontaine de Vaucluse according to the evapotranspiration model used, and to compare the simulations with the observations. The simulations depend on the used evapotranspiration model. Fig. B.1, the simulated discharge with KaRaMel + ET bucket model is symbolized by Qbucket, the simulated discharge with KaRaMel + SimpKcET is symbolized by Qsimpkcet and daily discharge observations are symbolized by Qobs. The simulated Fontaine de Vaucluse discharges time series are compared to the observed discharge over the 2009–215 period.

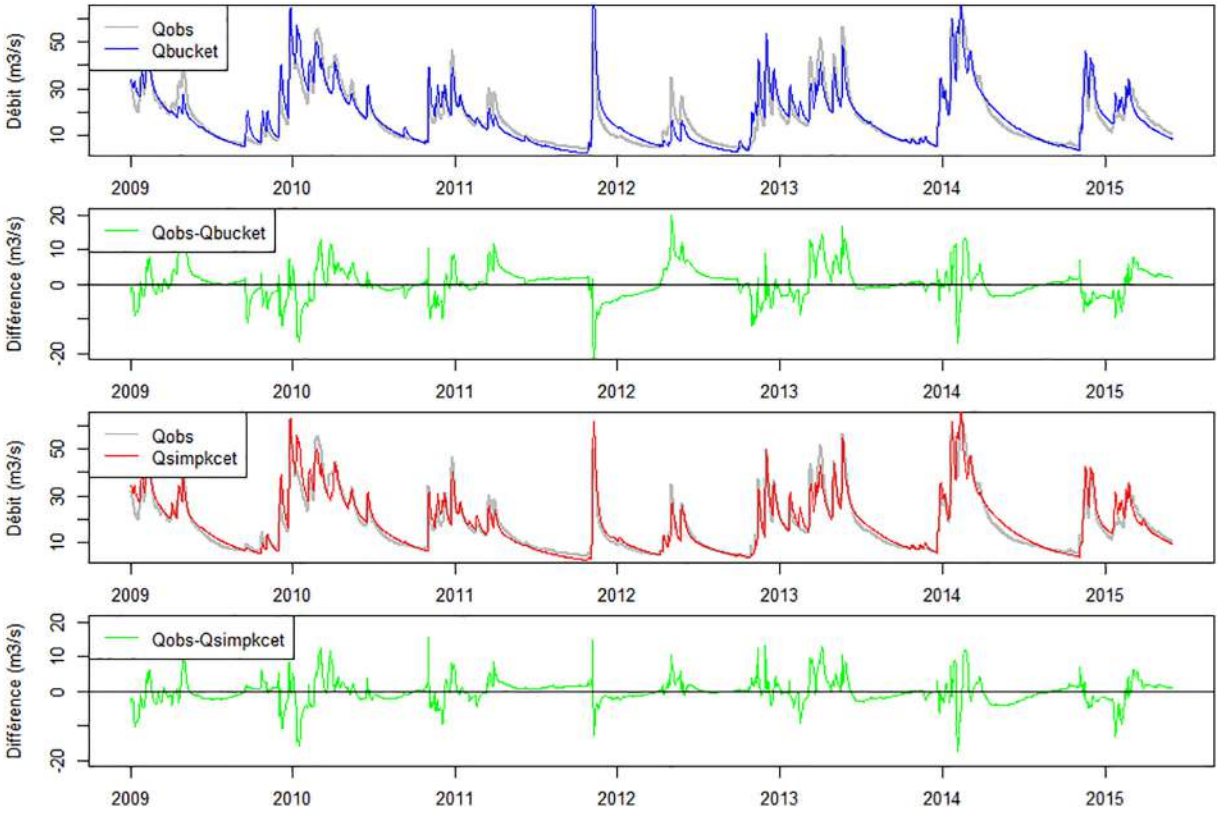

Fig. B-1. Time series of Fontaine de Vaucluse discharges: observed (Qobs) and simulated with KaRaMel + ET bucket model (Qbucket), with KaRaMel + SimpKcET (Qsimpkcet).

Appendix C. Selected area of the impluvium of Fontaine de Vaucluse with almost homogeneous land cover

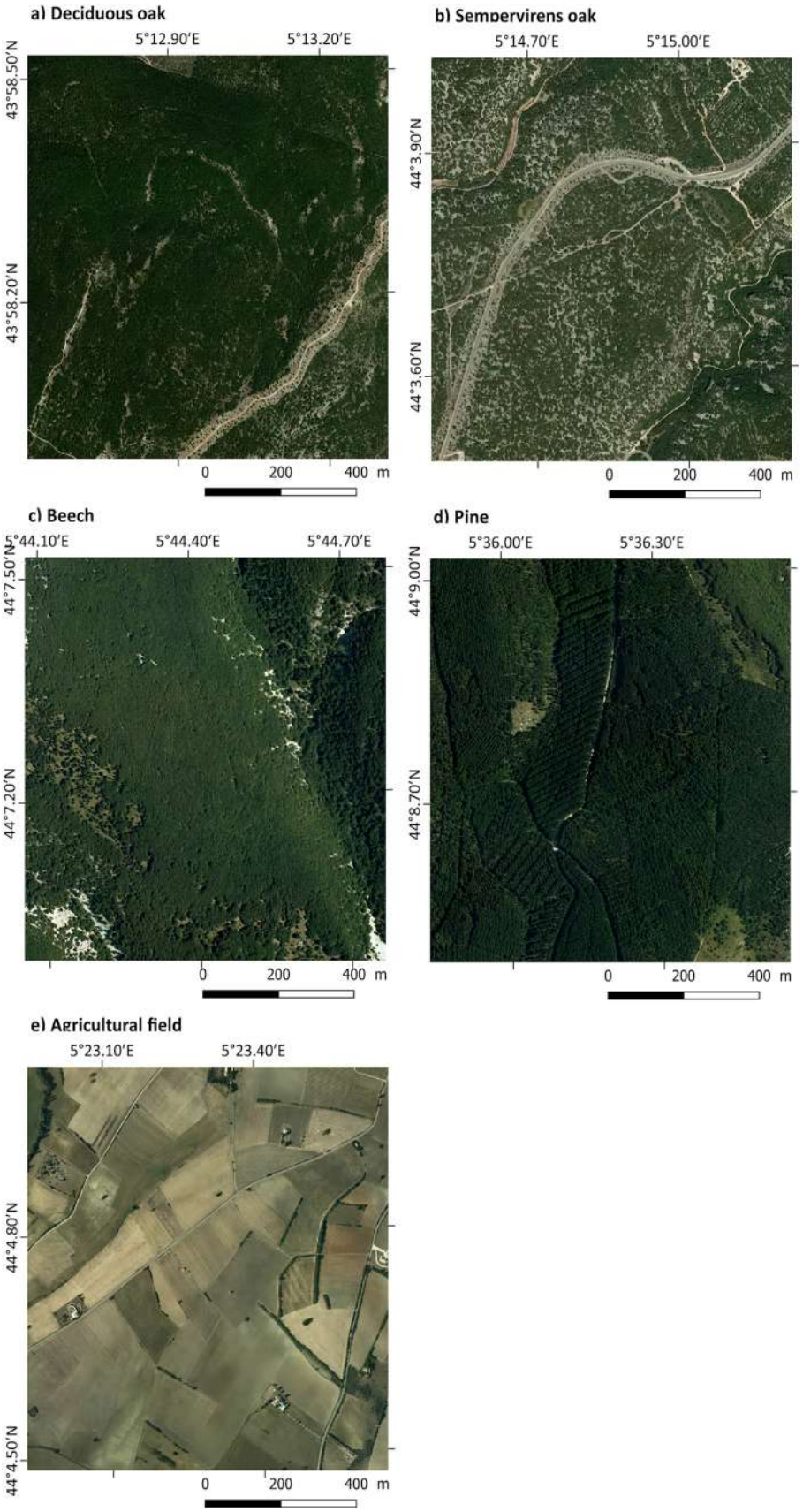

Fig. C-1. The areas presented are characterized by a homogeneous vegetation cover at the mesh scale of KaRaMel: a) oak forest Deciduous, b) oak forest Sempervirens, c) beech forest, d) pine forest and e) cultivated fields.

Appendix D. Details on climate of the studied sites

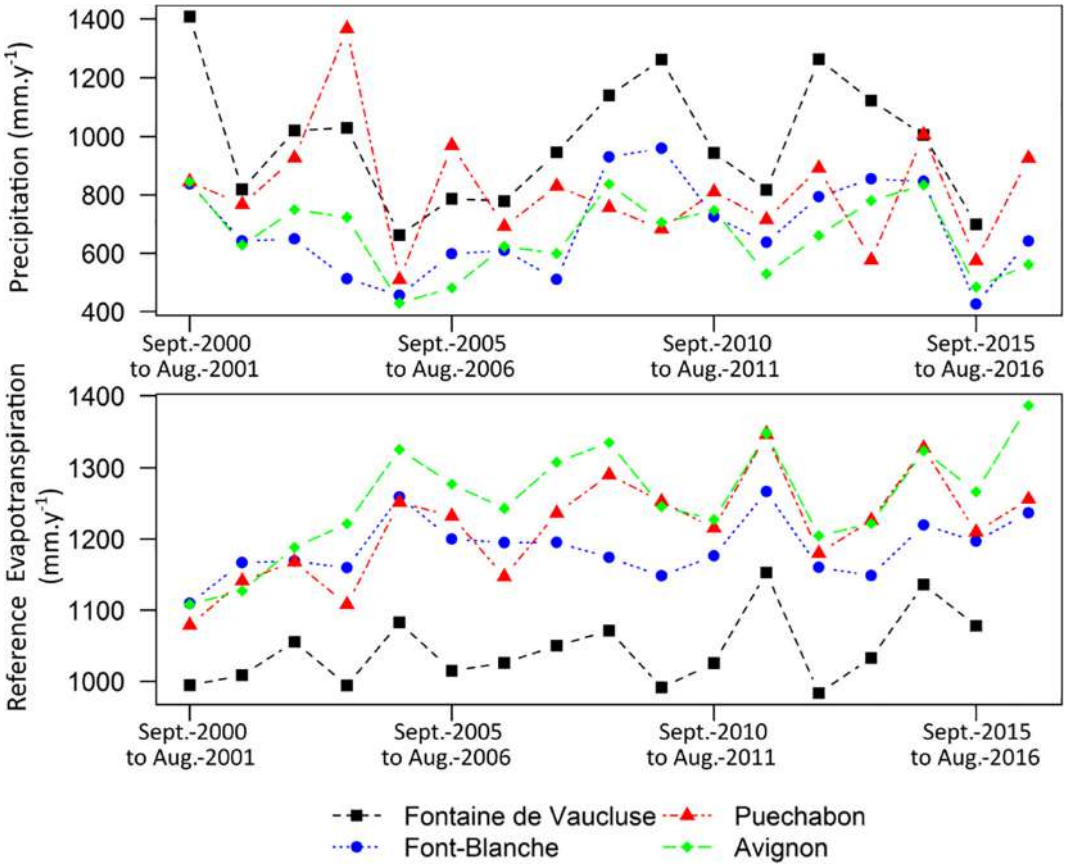

Fig. D-1. Annual precipitation and reference evapotranspiration of studied sites (hydrological year from September to August).

The climate data came from the SAFRAN product of METEO-FRANCE, the French meteorological service [Durand et al., 2009; Quintana-Seguí et al., 2008]. SAFRAN is a weather data source available over France on a grid of 8 km by 8 km at the daily scales starting in 1958. SAFRAN product is a surface - atmosphere reanalysis that is built by combining atmospheric model simulations to ground data, we used precipitation and reference evapotranspiration data. SAFRAN reference evapotranspiration was calculated with the Penman-Monteith equation from solar radiation, atmospheric radiation, air temperature, air humidity and wind speed. As in Allen et al. [1998] for the FAO56 methodology, the reference evapotranspiration is estimated for a well-irrigated grass canopy according to the climatic conditions. However, parameters used in the implementation of the Penman-Monteith equation by METEO-FRANCE are slightly different from those of Allen et al. [1998], in particular with lower albedo (0.20 instead of 0.23) and lower surface resistance (60 $m.s^{-1}$ instead of 70 $m.s^{-1}$). This resulted in a higher potential ET than with the FAO56 methodology.

The four test sites are situated in the typical Mediterranean climate zone, after Köppen-Geiger climate classification updated by Beck et al. [2018]. Winter is wet and cool, summer is hot and dry. Most of the precipitations occur during autumn and winter. Thus, climate is characterized by frequent summer droughts lasting at least for 2 months and regularly up to 4 months. Mean annual precipitation and temperatures of hydrological year from September 2000 to August 2016 are (Fig. D-1): 981 mm and 10 °C over Fontaine de Vaucluse watershed, 686 mm and 14 °C in Font-Blanche, 807 mm and 14.5 °C in Puechabon, 666 mm and 15 °C in Avignon. Mean annual reference evapotranspiration is 1043 mm for Fontaine de Vaucluse watershed, 1184 mm in Font-Blanche, 1213 mm in Puechabon and 1248 mm in Avignon.

The difference in climatic demands between these sites is mainly related to temperatures. It is interesting to note that years with lowest precipitation amounts are characterized by highest reference evapotranspiration values. The interannual variability of reference evapotranspiration is very low (maximum range around 200 mm) compared to precipitation (maximum range around 700 mm). However, an increasing trend is visible, which is mainly related to the elevation of air temperature, in agreement with the 1 $mm.year^{-1}$ to 2.5 $mm.year^{-1}$ observed over the lower Rhone Valley [Olioso et al., 2013]. No specific trends are detectable on the rain evolution.

References

Allard, V., Ourcival, J.M., Rambal, S., Joffre, R., Rocheteau, A., 2008. Seasonal and annual variation of carbon exchange in an evergreen Mediterranean forest in southern France. Glob. Chang. Biol. 14, 714–725. https://doi.org/10.1111/j.1365-2486.2008.01539.x.

Allen, R.G., Pereira, L.S., 2009. Estimating crop coefficients from fraction of ground cover and height. Irrig. Sci. 28, 17–34. https://doi.org/10.1007/s00271-009-0182-z.

Allen, R.G., Pereira, L.S., Raes, D., Smith, M., 1998. FAO Irrigation and drainage paper No. 56. Rome: Food and Agriculture Organization of the United Nations 56, e156.

Allen, R.G., Pruitt, W.O., Raes, D., Smith, M., Pereira, L.S., 2005. Estimating evaporation from bare soil and the crop coefficient for the initial period using common soils information. J. Irrig. Drain. Eng. 131, 14–23. https://doi.org/10.1061/(ASCE)0733-9437(2005)131:1(14).

Allies, A., Demarty, J., Olioso, A., Bouzou Moussa, I., Issoufou, H.B.-A., Velluet, C., Bahir, M., Maïnassara, I., Oï, M., Chazarin, J.-P., Cappelaere, B., 2020. Evapotranspiration

estimation in the Sahel using a new ensemble-contextual method. Remote Sens. 12, 380. https://doi.org/10.3390/rs12030380.
AnaEE, 2021. Analysis and Experiments on Ecosystems. https://www.anaee-france.fr/en/. (Accessed 1 July 2021).
Ardia, D., Boudt, K., Carl, P., Mullen, K., M., Peterson, B., G., 2011. Differential Evolution with DEoptim. The R Journal 3, 27. doi:10.32614/RJ-2011-005.
Arrouays, D., Leenaars, J.G.B., Richer-de-Forges, A.C., Adhikari, K., Ballabio, C., Greve, M., Grundy, M., Guerrero, E., Hempel, J., Hengl, T., Heuvelink, G., Batjes, N., Carvalho, E., Hartemink, A., Hewitt, A., Hong, S.-Y., Krasilnikov, P., Lagacherie, P., Lelyk, G., Libohova, Z., Lilly, A., McBratney, A., McKenzie, N., Vasquez, G.M., Mulder, V.L., Minasny, B., Montanarella, L., Odeh, I., Padarian, J., Poggio, L., Roudier, P., Saby, N., Savin, I., Searle, R., Solbovoy, V., Thompson, J., Smith, S., Sulaeman, Y., Vintila, R., Rossel, R.V., Wilson, P., Zhang, G.-L., Swerts, M., Oorts, K., Karklins, A., Feng, L., Ibelles Navarro, A.R., Levin, A., Laktionova, T., Dell'Acqua, M., Suvannang, N., Ruam, W., Prasad, J., Patil, N., Husnjak, S., Pásztor, L., Okx, J., Hallett, S., Keay, C., Farewell, T., Lilja, H., Juilleret, J., Marx, S., Takata, Y., Kazuyuki, Y., Mansuy, N., Panagos, P., Van Liedekerke, M., Skalsky, R., Sobocka, J., Kobza, J., Eftekhari, K., Alavipanah, S.K., Moussadek, R., Badraoui, M., Da Silva, M., Paterson, G., Gonçalves, M. da C., Theocharopoulos, S., Yemefack, M., Tedou, S., Vrscaj, B., Grob, U., Kozák, J., Boruvka, L., Dobos, E., Taboada, M., Moretti, L., Rodriguez, D., 2017. Soil legacy data rescue via GlobalSoilMap and other international and national initiatives. GeoResJ 14, 1–19. doi:https://doi.org/10.1016/j.grj.2017.06.001.
Bailly-Comte, V., Borrell-Estupina, V., Jourde, H., Pistre, S., 2012. A conceptual semidistributed model of the coulazou river as a tool for assessing surface water-karst groundwater interactions during flood in mediterranean ephemeral rivers. Wat. Resour. Res. 48 (9). https://doi.org/10.1029/2010WR010072.
Baldocchi, D., Falge, E., Gu, L., Olson, R., Hollinger, D., Running, S., Anthoni, P., Bernhofer, Ch., Davis, K., Evans, R., Fuentes, J., Goldstein, A., Katul, G., Law, B., Lee, X., Malhi, Y., Meyers, T., Munger, W., Oechet, W., Paw U, K.T., Pilegaard, K., Schmid, H.P., Valentini, R., Verma, S., Vesala, T., Wilson, K., Wofsy, S., 2001. FLUXNET: a new tool to study the temporal and spatial variability of ecosystem-scale carbon dioxide, water vapor, and energy flux densities. Bull. Am. Meteorol. Soc. 82, 2415–2434. doi:10.1175/1520-0477(2001)082<2415:FANTTS>2.3.CO;2.
Baret, F., Weiss, M., Verger, A., & Smets, B. 2013. ATBD for LAI, fAPAR And Fcover From Proba-V Products At 300m Resolution (Geov3). IMAGINES_RP2.1_ATBD-LAI300M, ISSUE 1.73, EC Proposal Reference N° FP7–311766.
Bausch, W.C., 1993. Soil background effects on reflectance-based crop coefficients for corn. Remote Sens. Environ. 46, 213–222. https://doi.org/10.1016/0034-4257(93)90096-G.
Bausch, W.C., Neale, C.M.U., 1987. Crop Coefficients Derived from Reflected Canopy Radiation: A Concept. Transactions of the ASAE 30, 703–0709. doi:10.13031/2013.30463.
Beck, H.E., Zimmermann, N.E., McVicar, T.R., Vergopolan, N., Berg, A., Wood, E.F., 2018. Present and future Köppen-Geiger climate classification maps at 1-km resolution. Sci Data 5, 180214. https://doi.org/10.1038/sdata.2018.214.
Bottner, P., 1971. Evolution des sols en milieu carbonaté. Université Montpellier, La pédogenèse sur les roches calcaires dans une séquence bioclimatique méditerranéo-alpine du Sud de la France.
Breshears, D.D., Cobb, N.S., Rich, P.M., Price, K.P., Allen, C.D., Balice, R.G., Romme, W.H., Kastens, J.H., Floyd, M.L., Belnap, J., Anderson, J.J., Myers, O.B., Meyer, C.W., 2005. Regional vegetation die-off in response to global-change-type drought. Proc. Natl. Acad. Sci. 102, 15144–15148. https://doi.org/10.1073/pnas.0505734102.
Brutsaert, W., 1982. Evaporation into the Atmosphere: Theory, History, and Applications. Kluwer, Dordrecht.
CARBOEUROPE-IP, 2019. Assessment of the european terrestrial carbon balance. URL: http://www.carboeurope.org. (Accessed 24 December 2020).
Carlson, T.N., Ripley, D.A., 1997. On the relation between NDVI, fractional vegetation cover, and leaf area index. Remote Sens. Environ. 62, 241–252. https://doi.org/10.1016/S0034-4257(97)00104-1.
Carpintero, E., González-Dugo, M.P., Jódar, J., Martos-Rosillo, S., 2018. Use of canopy coefficients obtained from satellite data to estimate evapotranspiration over high mountain Mediterranean watersheds. Proc. IAHS 380, 23–28. https://doi.org/10.5194/piahs-380-23-2018.
Carrière, S.D., Chalikakis, K., Danquigny, C., Davi, H., Mazzilli, N., Ollivier, C., Emblanch, C., 2016. The role of porous matrix in water flow regulation within a karst unsaturated zone: an integrated hydrogeophysical approach. Hydrogeol. J. https://doi.org/10.1007/s10040-016-1425-8.
Carrière, S.D., Ruffault, J., Cakpo, C.B., Olioso, A., Doussan, C., Simioni, G., Chalikakis, K., Patris, N., Davi, H., MartinSt-Paul, N.K., 2020a. Intra-specific variability in deep water extraction between trees growing on a Mediterranean karst. J. Hydrol. 125428. https://doi.org/10.1016/j.jhydrol.2020.125428.
Carrière, S.D., St-Paul, N.K.M., Cakpo, C.B., Patris, N., Gillon, M., Chalikakis, K., Doussan, C., Olioso, A., Babic, M., Jouineau, A., Simioni, G., Davi, H., 2020b. The role of deep vadose zone water in tree transpiration during drought periods in karst settings – insights from isotopic tracing and leaf water potential. Sci. Total Environ. 699, 134332. https://doi.org/10.1016/j.scitotenv.2019.134332.
Charlier, J.-B., Bertrand, C., Mudry, J., 2012. Conceptual hydrogeological model of flow and transport of dissolved organic carbon in a small Jura karst system. J. Hydrol. 460–461, 52–64. https://doi.org/10.1016/j.jhydrol.2012.06.043.
Charlier, J.-B., Ladouche, B., Maréchal, J.-C., 2015. Identifying the impact of climate and anthropic pressures on karst aquifers using wavelet analysis. J. Hydrol. 523, 610–623. https://doi.org/10.1016/j.jhydrol.2015.02.003.
Chen, Z., Auler, A.S., Bakalowicz, M., Drew, D., Griger, F., Hartmann, J., Jiang, G., Moosdorf, N., Richts, A., Stevanovic, Z., Veni, G., Goldscheider, N., 2017. The world karst aquifer mapping project: concept, mapping procedure and map of Europe. Hydrogeol. J. 25, 771–785. https://doi.org/10.1007/s10040-016-1519-3.
Choudhury, B.J., Ahmed, N.U., Idso, S.B., Reginato, R.J., Daughtry, C.S.T., 1994. Relations between Evaporation Coefficients and Vegetation Indices Studied by Model Simulations. Remote sens. environ. 1–17. doi:10.1016/0034-4257(94)90090-6.
Chu, H., Baldocchi, D.D., John, R., Wolf, S., Reichstein, M., 2017. Fluxes all of the time? A primer on the temporal representativeness of FLUXNET: fluxes all of the time? Journal of Geophysical Research: Biogeosciences 122, 289–307. https://doi.org/10.1002/2016JG003576.
Clobert, J., Chanzy, A., Le Galliard, J.-F., Chabbi, A., Greiveldinger, L., Caquet, T., Loreau, M., Mougin, C., Pichot, C., Roy, J., Saint-André, L., 2018. How to integrate experimental research approaches in ecological and environmental studies: AnaEE France as an example. Front. Ecol. Evol. 6, 43. https://doi.org/10.3389/fevo.2018.00043.
COPERNICUS Land Monitoring Service. https://land.copernicus.eu/global/products/fcover. (Accessed 24 December 2020).
Cramer, W., Bondeau, A., Woodward, F.I., Prentice, I.C., Betts, R.A., Brovkin, V., Cox, P.M., Fisher, V., Foley, J.A., Friend, A.D., Kucharik, C., Lomas, M.R., Ramankutty, N., Sitch, S., Smith, B., White, A., Young-Molling, C., 2001. Global response of terrestrial ecosystem structure and function to CO2 and climate change: results from six dynamic global vegetation models. Glob. Chang. Biol. 7, 357–373. https://doi.org/10.1046/j.1365-2486.2001.00383.x.
Delaigue, O., Thirel, G., Bourgin, F., Coron, L., 2018. Latest Developments of the airGR Rainfall-runoff Modelling R Package: New Calibration Procedures and Other Features.
Doorenbos, J., Pruitt, W.O., 1977. Guidelines for predicting crop water requirements. Food and Agriculture organization of the united nation. Irrigation and Drainage paper 24, 154.
Durand, Y., Laternser, M., Giraud, G., Etchevers, P., Lesaffre, B., Mérindol, L., 2009. Reanalysis of 44 Yr of climate in the French Alps (1958–2002): methodology, model validation, climatology, and trends for air temperature and precipitation. J. Appl. Meteorol. Climatol. 48, 429–449. https://doi.org/10.1175/2008JAMC1808.1.
EARTHDATA, 2019. The earth observing system data and information system. URL: https://search.earthdata.nasa.gov/search. (last accessed: 24.12.2020).
Farahani, H.J., Howell, T.A., Shuttleworth, W.J., Bausch, W.C., 2007. Evapotranspiration: progress in measurement and modeling in agriculture. Trans. ASABE 50 (5), 1627–1638.
Fisher, J.B., Melton, F., Middleton, E., Hain, C., Anderson, M., Allen, R., McCabe, M.F., Hook, S., Baldocchi, D., Townsend, P.A., Kilic, A., Tu, K., Miralles, D.D., Perret, J., Lagouarde, J.-P., Waliser, D., Purdy, A.J., French, A., Schimel, D., Famiglietti, J.S., Stephens, G., Wood, E.F., 2017. The future of evapotranspiration: global requirements for ecosystem functioning, carbon and climate feedbacks, agricultural management, and water resources. Water Resour. Res. 9.
Fleury, P., Plagnes, V., Bakalowicz, M., 2007. Modelling of the functioning of karst aquifers with a reservoir model: application to Fontaine de Vaucluse (South of France). J. Hydrol. 345, 38–49. https://doi.org/10.1016/j.jhydrol.2007.07.014.
Ford, D., Williams, P., 2007. Karst Hydrogeology and Geomorphology 30.
Gallego-Elvira, B., Olioso, A., Mira, M., Castillo, S.R.-, Boulet, G., Marloie, O., Garrigues, S., Courault, D., Weiss, M., Chauvelon, P., Boutron, O., 2013. EVASPA (EVapotranspiration Assessment from SPAce) tool: an overview. Procedia Environ. Sci. 19, 303–310. doi:https://doi.org/10.1016/j.proenv.2013.06.035.
Gao, L., Wang, X., Johnson, B.A., Tian, Q., Wang, Y., Verrelst, J., Mu, X., Gu, X., 2020. Remote sensing algorithms for estimation of fractional vegetation cover using pure vegetation index values: a review. ISPRS J. Photogramm. Remote Sens. 159, 364–377. https://doi.org/10.1016/j.isprsjprs.2019.11.018.
Garrigues, S., Olioso, A., Calvet, J.C., Martin, E., Lafont, S., Moulin, S., Chanzy, A., Marloie, O., Buis, S., Desfonds, V., Bertrand, N., Renard, D., 2015. Evaluation of land surface model simulations of evapotranspiration over a 12-year crop succession: impact of soil hydraulic and vegetation properties. Hydrol. Earth Syst. Sci. 19, 3109–3131. https://doi.org/10.5194/hess-19-3109-2015.
Garrigues, S., Boone, A., Decharme, B., Olioso, A., Albergel, C., Calvet, J.-C., Moulin, S., Buis, S., Martin, E., 2018. Impacts of the soil water transfer parameterization on the simulation of evapotranspiration over a 14-year Mediterranean crop succession. J. Hydrometeorol. 19, 3–25. https://doi.org/10.1175/JHM-D-17-0058.1.
Girard, F., Vennetier, M., Guibal, F., Corona, C., Ouarmim, S., Herrero, A., 2012. Pinus halepensis Mill. crown development and fruiting declined with repeated drought in Mediterranean France. Eur. J. For. Res. 131, 919–931. https://doi.org/10.1007/s10342-011-0565-6.
Godard, V., Ollivier, V., Bellier, O., Miramont, C., Shabanian, E., Fleury, J., Benedetti, L., Guillou, V., 2016. Weathering-limited hillslope evolution in carbonate landscapes. Earth Planet. Sci. Lett. 446, 10–20. https://doi.org/10.1016/j.epsl.2016.04.017.
González-Dugo, M.P., Mateos, L., 2008. Spectral vegetation indices for benchmarking water productivity of irrigated cotton and sugarbeet crops. Agric. Water Manag. 95, 48–58. https://doi.org/10.1016/j.agwat.2007.09.001.
Grippa, M., Kergoat, L., Boone, A., Peugeot, C., Demarty, J., Cappelaere, B., Gal, L., Hiernaux, P., Mougin, E., Ducharne, A., Dutra, E., Anderson, M., Hain, C., ALMIP2 Working Group, 2017. Modeling surface runoff and water fluxes over contrasted soils in the pastoral Sahel: evaluation of the ALMIP2 land surface models over the Gourma Region in Mali. J. Hydrometeorol. 18, 1847–1866. https://doi.org/10.1175/JHM-D-16-0170.1.
Gupta, H.V., Kling, H., Yilmaz, K.K., Martinez, G., 2009. Decomposition of the mean squared error and NSE performance criteria: implications for improving hydrological modelling. J. Hydrol. 377, 80–91. https://doi.org/10.1016/j.jhydrol.2009.08.003.
Hargreaves, G.H., Allen, R.G., 2003. History and evaluation of Hargreaves evapotranspiration equation. J. Irrig. Drain. Eng. 129, 53–63. https://doi.org/10.1061/(ASCE)0733-9437(2003)129:1(53).
Hargreaves, G. H., & Samani, Z. A. (1985). Reference crop evapotranspiration from temperature. Applied engineering in agriculture, 1(2), 96-99. doi: 10.13031/2013.26773.
Hartmann, A., Lange, J., Weiler, M., Arbel, Y., Greenbaum, N., 2012. A new approach to model the spatial and temporal variability of recharge to karst aquifers. Hydrol. Earth Syst. Sci. 16, 2219–2231. https://doi.org/10.5194/hess-16-2219-2012.

Hartmann, A., Goldscheider, N., Wagener, T., Lange, J., Weiler, M., 2014. Karst water resources in a changing world: review of hydrological modeling approaches. Rev. Geophys. 52, 218–242. https://doi.org/10.1002/2013RG000443.

Hartmann, A., Gleeson, T., Rosolem, R., Pianosi, F., Wada, Y., Wagener, T., 2015. A large-scale simulation model to assess karstic groundwater recharge over Europe and the Mediterranean. Geosci. Model Dev. 8, 1729–1746. https://doi.org/10.5194/gmd-8-1729-2015.

Heilman, J.L., Heilman, W.E., Moore, D.G., 1982. Evaluating the crop coefficient using spectral Reflectance1. Agron. J. 74, 967. https://doi.org/10.2134/agronj1982.00021962007400060010x.

Helman, D., Givati, A., Lensky, I.M., 2015. Annual evapotranspiration retrieved from satellite vegetation indices for the eastern Mediterranean at 250 m spatial resolution. Atmos. Chem. Phys. 15, 12567–12579. https://doi.org/10.5194/acp-15-12567-2015.

Hu, K., Chen, H., Nie, Y., Wang, K., 2015. Seasonal recharge and mean residence times of soil and epikarst water in a small karst catchment of southwest China. Sci. Rep. 5, 10215. https://doi.org/10.1038/srep10215.

Huete, A.R., 1988. A soil-adjusted vegetation index (SAVI). Remote Sens. Environ. 25, 295–309. https://doi.org/10.1016/0034-4257(88)90106-X.

Huete, A., Justice, C., Liu, H., 1994. Development of vegetation and soil indices for MODIS-EOS. Remote Sens. Environ. 49, 224–234.

Huete, A., Didan, K., Miura, T., Rodriguez, E.P., Gao, X., Ferreira, L.G., 2002. Overview of the radiometric and biophysical performance of the MODIS vegetation indices. Remote Sens. Environ. 83, 195–213.

Huete, A., Didan, K., van Leeuwen, W., Miura, T., Glenn, E., 2010. MODIS vegetation indices. In: Ramachandran, B., Justice, C.O., Abrams, M.J. (Eds.), Land Remote Sensing and Global Environmental Change. Springer New York, New York, NY, pp. 579–602 https://doi.org/10.1007/978-1-4419-6749-7_26.

ICOS, 2021. Integrated Carbon Observation System, monitoring networks of the greenhouse gases in the atmosphere, oceans and continents. https://www.icos-france.fr/en. (Accessed 1 July 2021).

Jensen, M.E., Burman, R.D., Allen, R.G., 1990. Evapotranspiration and Irrigation Water Requirements. ASCE.

Jódar, J., Carpintero, E., Martos-Rosillo, S., Ruiz-Constán, A., Marín-Lechado, C., Cabrera-Arrabal, J.A., Navarrete-Mazariegos, E., González-Ramón, A., Lambán, L.J., Herrera, C., González-Dugo, M.P., 2018. Combination of lumped hydrological and remote-sensing models to evaluate water resources in a semi-arid high altitude ungauged watershed of Sierra Nevada (Southern Spain). Sci. Total Environ. 625, 285–300. https://doi.org/10.1016/j.scitotenv.2017.12.300.

Jung, H.C., Getirana, A., Arsenault, K.R., Holmes, T.R.H., McNally, A., 2019. Uncertainties in evapotranspiration estimates over West Africa. Remote Sens. 11, 892. https://doi.org/10.3390/rs11080892.

Kandasamy, S., Baret, F., Verger, A., Neveux, P., Weiss, M., 2013. A comparison of methods for smoothing and gap filling time series of remote sensing observations-application to MODIS LAI products. Biogeosciences 10 (6), 4055–4071. https://doi.org/10.5194/bg-10-4055-2013.

Kimball, B., Boote, K., Hatfield, J., Ahuja, L., Stockle, C., Archontoulis, S., Baron, C., Basso, B., Bertuzzi, P., Chen, M., Constantin, J., Derying, D., Dumont, B., Durand, J.-L., Ewert, F., Gaiser, T., Gayler, S., GRIFFIS, T., Hoffmann, M., Jiang, Q., Kim, S.-H., Lizaso, J., Moulin, S., Nendel, C., Parker, P., Palosuo, T., Priesack, E., Qi Z., Z., Srivastava, A., Stella, T., Tao, F., Thorp, K., Timlin, D., Twine, T., Webber, H., Willaume, M., Williams, K., 2017. Prediction of Evapotranspiration and Yields of Maize: An Inter-comparison among 31 Maize Models, in: Meeting of Working Group *Medicago sativa*. Tampa , United States, p. 1. https://hal.inria.fr/hal-02950305.

Kite, G.W., Kouwen, N., 1992. Watershed modeling using land classification. Water Resour. Res. 28, 3193–3200. https://doi.org/10.1029/92WR01819.

Kumar, P., Foufoula-Georgiou, E., 1997. Wavelet analysis for geophysical applications. Rev. Geophys. 35, 385–412. https://doi.org/10.1029/97RG00427.

Labat, D., 2005. Recent advances in wavelet analyses: part 1. A review of concepts. Journal of Hydrology 314, 275–288. https://doi.org/10.1016/j.jhydrol.2005.04.003.

Labat, D., 2010. Cross wavelet analyses of annual continental freshwater discharge and selected climate indices. J. Hydrol. 385, 269–278. https://doi.org/10.1016/j.jhydrol.2010.02.029.

Labat, D., Ababou, R., Mangin, A., 2000a. Rainfall–runoff relations for karstic springs. Part I: convolution and spectral analyses. Journal of Hydrology 238, 123–148. https://doi.org/10.1016/S0022-1694(00)00321-8.

Labat, D., Ababou, R., Mangin, A., 2000b. Rainfall–runoff relations for karstic springs. Part II: continuous wavelet and discrete orthogonal multiresolution analyses. Journal of hydrology 238, 149–178. https://doi.org/10.1016/S0022-1694(00)00322-X.

Ladouche, B., Marechal, J.-C., Dorfliger, N., 2014. Semi-distributed lumped model of a karst system under active management. J. Hydrol. 509, 215–230. https://doi.org/10.1016/j.jhydrol.2013.11.017.

Li, W., Weiss, M., Waldner, F., Defourny, P., Demarez, V., Morin, D., Hagolle, O., Baret, F., 2015. A generic algorithm to estimate LAI, FAPAR and FCOVER variables from SPOT4_HRVIR and Landsat sensors: evaluation of the consistency and comparison with ground measurements. Remote Sens. 7, 15494–15516. https://doi.org/10.3390/rs71115494.

Lin, Y.-S., Medlyn, B.E., Duursma, R.A., Prentice, I.C., Wang, H., Baig, S., Eamus, D., de Dios, V.R., Mitchell, P., Ellsworth, D.S., de Beeck, M.O., Wallin, G., Uddling, J., Tarvainen, L., Linderson, M.-L., Cernusak, L.A., Nippert, J.B., Ocheltree, T.W., Tissue, D.T., Martin-StPaul, N.K., Rogers, A., Warren, J.M., De Angelis, P., Hikosaka, K., Han, Q., Onoda, Y., Gimeno, T.E., Barton, C.V.M., Bennie, J., Bonal, D., Bosc, A., Löw, M., Macinins-Ng, C., Rey, A., Rowland, L., Setterfield, S.A., Tausz-Posch, S., Zaragoza-Castells, J., Broadmeadow, M.S.J., Drake, J.E., Freeman, M., Ghannoum, O., Hutley, L.B., Kelly, J.W., Kikuzawa, K., Kolari, P., Koyama, K., Limousin, J.-M., Meir, P., Lola da Costa, A.C., Mikkelsen, T.N., Salinas, N., Sun, W., Wingate, L., 2015. Optimal stomatal behaviour around the world. Nat. Clim. Chang. 5, 459. https://doi.org/10.1038/nclimate2550.

Liu, S., Huang, S., Xie, Y., Wang, H., Huang, Q., Leng, G., Li, P., Wang, L., 2019. Spatial-temporal changes in vegetation cover in a typical semi-humid and semi-arid region in China: changing patterns, causes and implications. Ecol. Indic. 98, 462–475. https://doi.org/10.1016/j.ecolind.2018.11.037.

Marie, G., Simioni, G., 2014. Extending the use of ecological models without sacrificing details: a generic and parsimonious meta-modelling approach. Methods Ecol. Evol. 5, 934–943. https://doi.org/10.1111/2041-210X.12250.

Martens, B., Miralles, D.G., Lievens, H., Fernández-Prieto, D., Beck, H.E., Dorigo, W.A., Verhoest, N.E.C., 2017. GLEAM v3: satellite-based land evaporation and root-zone soil moisture. Geosci. Model Dev. 23. https://doi.org/10.5194/gmd-10-1903-2017.

McBratney, A.B., Mendonça Santos, M.L., Minasny, B., 2003. On digital soil mapping. Geoderma 117, 3–52. https://doi.org/10.1016/S0016-7061(03)00223-4.

McDonald, J.E., 1961. On the ratio of evaporation to precipitation. Bull. Am. Meteorol. Soc. 42, 185–189. https://doi.org/10.1175/1520-0477-42.3.185.

Melton, F.S., Johnson, L.F., Lund, C.P., Pierce, L.L., Michaelis, A.R., Hiatt, S.H., Guzman, A., Adhikari, D.D., Purdy, A.J., Rosevelt, C., Votava, P., Trout, T.J., Temesgen, B., Frame, K., Sheffner, E.J., Nemani, R.R., 2012. Satellite irrigation management support with the terrestrial observation and prediction system: a framework for integration of satellite and surface observations to support improvements in agricultural water resource management. IEEE Journal of Selected Topics in Applied Earth Observations and Remote Sensing 5, 1709–1721. https://doi.org/10.1109/JSTARS.2012.2214474.

Messerschmid, C., Sauter, M., Lange, J., 2020. Field-based estimation and modelling of distributed groundwater recharge in a Mediterranean karst catchment, Wadi Natuf. West Bank. Hydrol. Earth Syst. Sci. 24, 887–917. https://doi.org/10.5194/hess-24-887-2020.

Moreira, A.A., Ruhoff, A.L., Roberti, D.R., Souza, V. de A., da Rocha, H.R., Paiva, R.C.D. de, 2019. Assessment of terrestrial water balance using remote sensing data in South America. J. Hydrol. 575, 131–147. doi:https://doi.org/10.1016/j.jhydrol.2019.05.021.

Mu, Q., Heinsch, F.A., Zhao, M., Running, S.W., 2007. Development of a global evapotranspiration algorithm based on MODIS and global meteorology data. Remote Sens. Environ. 111, 519–536. https://doi.org/10.1016/j.rse.2007.04.015.

Mu, Q., Zhao, M., Running, S.W., 2011. Improvements to a MODIS global terrestrial evapotranspiration algorithm. Remote Sens. Environ. 115, 1781–1800. https://doi.org/10.1016/j.rse.2011.02.019.

Nourtier, M., Chanzy, A., Cailleret, M., Yingge, X., Huc, R., Davi, H., 2014. Transpiration of silver Fir (Abies alba mill.) during and after drought in relation to soil properties in a Mediterranean mountain area. Ann. For. Sci. 71, 683–695. https://doi.org/10.1007/s13595-012-0229-9.

Olioso, A., Lecerf, R., Chanzy, A., Ruget, F., Huard, F.F., Baillieux, A., Rossello, P., Lecharpentier, P., Trolard, F., Charron, F., Ruy, S., Alkassem-Alosman, M., Cognard-Plancq, A.-L., Seguin, B., Courault, D., Gallego-Elvira, B., Garrigues, S., 2013. Bilan hydrique des agrosystèmes de Crau face aux changements globaux., in: Ecologie et Conservation d'une Steppe Méditerranéenne. La Plaine de Crau.

Olioso, A., Ollivier, C., Martin-StPaul, N.K., Simioni, G., Weiss, M., Guillevic, P., Marloie, O., Carrière, S.D., Davi, H., Huard, F., 2019. Monitoring Vegetation Fraction Cover of French Mediterranean Forests for Evapotranspiration and Water Stress Mapping. Presented at the Living Planet Symposium, Milan.

Ollivier, C., 2019. Caractérisation et spatialisation de la recharge des hydrosystèmes karstiques: Application à l'aquifère de Fontaine de Vaucluse, France (PhD Thesis). Avignon Université, Avignon. https://tel.archives-ouvertes.fr/tel-02614260.

Ollivier, C., Mazzilli, N., Olioso, A., Chalikakis, K., Carrière, S.D., Danquigny, C., Emblanch, C., 2020. Karst recharge-discharge semi distributed model to assess spatial variability of flows. Sci. Total Environ. 703, 134368. https://doi.org/10.1016/j.scitotenv.2019.134368.

Oudin, L., 2004. Recherche d'un modèle d'évapotranspiration potentielle pertinent comme entrée d'un modèle pluie-débit global. ENGREF (AgroParisTech). https://pastel.archives-ouvertes.fr/pastel-00000931

Oudin, L., Hervieu, F., Michel, C., Perrin, C., Andréassian, V., Anctil, F., Loumagne, C., 2005a. Which potential evapotranspiration input for a lumped rainfall–runoff model? Part 2—towards a simple and efficient potential evapotranspiration model for rainfall–runoff modelling. J. Hydrol. 303, 290–306. https://doi.org/10.1016/j.jhydrol.2004.08.026.

Oudin, L., Michel, C., Anctil, F., 2005b. Which potential evapotranspiration input for a lumped rainfall-runoff model? Part 1—can rainfall-runoff models effectively handle detailed potential evapotranspiration inputs? J. Hydrol. 303, 275–289. https://doi.org/10.1016/j.jhydrol.2004.08.025.

Perrin, C., Michel, C., Andréassian, V., 2003. Improvement of a parsimonious model for streamflow simulation. J. Hydrol. 279, 275–289. https://doi.org/10.1016/S0022-1694(03)00225-7.

Pronk, M., Goldscheider, N., Zopfi, J., Zwahlen, F., 2009. Percolation and particle transport in the unsaturated zone of a karst aquifer. Ground Water 47, 361–369. https://doi.org/10.1111/j.1745-6584.2008.00509.x.

Qi, J., Chehbouni, A., Huete, A.R., Kerr, Y.H., Sorooshian, S., 1994. A modified soil adjusted vegetation index. Remote Sens. Environ. 48, 119–126. https://doi.org/10.1016/0034-4257(94)90134-1.

Quintana-Seguí, P., Le Moigne, P., Durand, Y., Martin, E., Habets, F., Baillon, M., Canellas, C., Franchisteguy, L., Morel, S., 2008. Analysis of near-surface atmospheric variables: validation of the SAFRAN analysis over France. J. Appl. Meteorol. Climatol. 47, 92–107. https://doi.org/10.1175/2007JAMC1636.1.

Rahman, M., Rosolem, R., 2017. Towards a simple representation of chalk hydrology in land surface modelling. Hydrol. Earth Syst. Sci. 21, 459–471. https://doi.org/10.5194/hess-21-459-2017.

Rambal, S., 1982. Variabilité des propriétés hydrodynamiques du sol à l'échelle d'un versant karstique. Presented at "the Variabilité spatiale des processus de transfert dans les sols", INRA, Avignon, pp. 201–211.

Rambal, S., 1984. Water balance and pattern of root water uptake by a Quercus coccifera L. evergreen scrub. Oecologia 18–25.
Rambal, S., 1992. Quercus ilex facing water stress: a functional equilibrium hypothesis. Vegetatio 99, 147–153. https://doi.org/10.1007/BF00118220.
Rambal, S., 1993. The differential role of mechanisms for drought resistance in a Mediterranean evergreen shrub: a simulation approach. Plant Cell Environ. 16, 35–44. https://doi.org/10.1111/j.1365-3040.1993.tb00842.x.
Rambal, S., Ourcival, J.-M., Joffre, R., Mouillot, F., Nouvellon, Y., Reichstein, M., Rocheteau, A., 2003. Drought controls over conductance and assimilation of a Mediterranean evergreen ecosystem: scaling from leaf to canopy. Glob. Chang. Biol. 9, 1813–1824. https://doi.org/10.1111/j.1365-2486.2003.00687.x.
Rambal, S., Lempereur, M., Limousin, J.M., Martin-StPaul, N.K., Ourcival, J.M., Rodríguez-Calcerrada, J., 2014. How drought severity constrains gross primary production (GPP) and its partitioning among carbon pools in a Quercus ilex coppice? Biogeosciences 11, 6855–6869. https://doi.org/10.5194/bg-11-6855-2014.
Rana, G., Katerji, N., 2000. Measurement and estimation of actual evapotranspiration in the field under Mediterranean climate: a review. Eur. J. Agron. 13, 125–153. https://doi.org/10.1016/S1161-0301(00)00070-8.
REVERB NASA web site, 2016. The earth observing system data and information system. URL: http://reverb.echo.nasa.gov/reverb/. (last accessed: 24.12.2020).
Rosch, A., Schmidbauer, H., 2019. WaveletComp 1.1: A guided tour through the R package 58.
Sang, Y.-F., 2013. A review on the applications of wavelet transform in hydrology time series analysis. Atmos. Res. 122, 8–15. https://doi.org/10.1016/j.atmosres.2012.11.003.
Sarrazin, F., Hartmann, A., Pianosi, F., Rosolem, R., Wagener, T., 2018. V2Karst V1.1: a parsimonious large-scale integrated vegetation–recharge model to simulate the impact of climate and land cover change in karst regions. Geosci. Model Dev. 11, 4933–4964. https://doi.org/10.5194/gmd-11-4933-2018.
Shen, H., Leblanc, M., Frappart, F., Seoane, L., O'Grady, D., Olioso, A., Tweed, S., 2017. A comparative study of GRACE with continental evapotranspiration estimates in Australian semi-arid and arid basins: sensitivity to climate variability and extremes. Water 9, 614. https://doi.org/10.3390/w9090614.
Shuttleworth, W.J., 2007. Putting the "vap" into evaporation. Hydrol. Earth Syst. Sci. 11, 210–244. https://doi.org/10.5194/hess-11-210-2007.
Shuttleworth, W.J., 2008. Evapotranspiration measurement methods. Southwest Hydrology 7, 22–23.
Simioni, G., Marie, G., Huc, R., 2016. Influence of vegetation spatial structure on growth and water fluxes of a mixed forest: results from the NOTG 3D model. Ecol. Model. 328, 119–135. https://doi.org/10.1016/j.ecolmodel.2016.02.004.
Torrence, C., Compo, G.P., 1998. A practical guide to wavelet analysis. Bull. Am. Meteorol. Soc. 79, 61–78. https://doi.org/10.1175/1520-0477(1998)079<0061:APGTWA>2.0.CO;2.
Trajkovic, S., 2005. Temperature-based approaches for estimating reference evapotranspiration. Journal of irrigation and drainage engineering. ASCE 131, 316–323. https://doi.org/10.1061/(ASCE)0733-9437(2005)131:4(316).
Tritz, S., Guinot, V., Jourde, H., 2011. Modelling the behaviour of a karst system catchment using non-linear hysteretic conceptual model. J. Hydrol. 397, 250–262. https://doi.org/10.1016/j.jhydrol.2010.12.001.
Vuolo, F., Żółtak, M., Pipitone, C., Zappa, L., Wenng, H., Immitzer, M., Weiss, M., Baret, F., Atzberger, C., 2016. Data service platform for Sentinel-2 surface reflectance and value-added products: system use and examples. Remote Sens. 8, 938. https://doi.org/10.3390/rs8110938.
Watlet, A., Kaufmann, O., Triantafyllou, A., Poulain, A., Chambers, J.E., Meldrum, P.I., Wilkinson, P.B., Hallet, V., Quinif, Y., Van Ruymbeke, M., Van Camp, M., 2018. Imaging groundwater infiltration dynamics in the karst vadose zone with long-term ERT monitoring. Hydrol. Earth Syst. Sci. 22, 1563–1592. https://doi.org/10.5194/hess-22-1563-2018.
Weiss, M., Baret, F., 2016. S2ToolBox Level 2 products: LAI, FAPAR, FCOVER. Version 1.1. INRA 53.
Weiss, M., Jacob, F., Baret, F., Pragnère, A., Bruchou, C., Leroy, M., Hautecœur, O., Prévot, L., Bruguier, N., 2002. Evaluation of kernel-driven BRDF models for the normalization of Alpilles/ReSeDA POLDER data. Agronomie 22, 531–536. https://doi.org/10.1051/agro:2002037.
Zambrano-Bigiarini, M., Rojas, R., 2013. A model-independent particle swarm optimisation software for model calibration. Environ. Model Softw. 43, 5–25. https://doi.org/10.1016/j.envsoft.2013.01.004.
Zhang, Z., Li, M., Si, B., Feng, H., 2018. Deep rooted apple trees decrease groundwater recharge in the highland region of the Loess Plateau, China. Sci. Total Environ. 622–623, 584–593. https://doi.org/10.1016/j.scitotenv.2017.11.230.